



UNIVERSITY OF LEEDS

This is a repository copy of *Environmental and trilobite diversity changes during the middle-late Cambrian SPICE event*.

White Rose Research Online URL for this paper:

<https://eprints.whiterose.ac.uk/196063/>

Version: Accepted Version

---

**Article:**

Zhang, L, Algeo, TJ, Zhao, L et al. (7 more authors) (2023) Environmental and trilobite diversity changes during the middle-late Cambrian SPICE event. GSA Bulletin. ISSN 0016-7606

<https://doi.org/10.1130/B36421.1>

---

This is an author produced version of an article published in GSA Bulletin. Uploaded in accordance with the publisher's self-archiving policy.

**Reuse**

This article is distributed under the terms of the Creative Commons Attribution (CC BY) licence. This licence allows you to distribute, remix, tweak, and build upon the work, even commercially, as long as you credit the authors for the original work. More information and the full terms of the licence here:

<https://creativecommons.org/licenses/>

**Takedown**

If you consider content in White Rose Research Online to be in breach of UK law, please notify us by emailing [eprints@whiterose.ac.uk](mailto:eprints@whiterose.ac.uk) including the URL of the record and the reason for the withdrawal request.



[eprints@whiterose.ac.uk](mailto:eprints@whiterose.ac.uk)  
<https://eprints.whiterose.ac.uk/>

1 Environmental and trilobite diversity changes during the  
2 middle-late Cambrian SPICE event  
3

4 Lei Zhang<sup>a\*</sup>, Thomas J. Algeo<sup>a, b, c</sup>, Laishi Zhao<sup>a\*</sup>, Tais W. Dahl<sup>a, d</sup>, Zhong-Qiang Chen<sup>a, b</sup>, Zihu  
5 Zhang<sup>e, f</sup>, Simon W. Poulton<sup>a, g</sup>, Nigel C. Hughes<sup>h</sup>, Xueqing Gou<sup>a</sup>, Chao Li<sup>e, f</sup>  
6

7 <sup>a</sup> State Key Laboratory of Geological Processes and Mineral Resources, China University of  
8 Geosciences, Wuhan 430074, China

9 <sup>b</sup> State Key Laboratory of Biogeology and Environmental Geology, China University of  
10 Geosciences, Wuhan 430074, China

11 <sup>c</sup> Department of Geosciences, University of Cincinnati, Cincinnati, OH 45221-0013, USA

12 <sup>d</sup> GLOBE Institute, University of Copenhagen, DK-1350 Copenhagen, Denmark

13 <sup>e</sup> State Key Laboratory of Oil and Gas Reservoir Geology and Exploitation & Institute of  
14 Sedimentary Geology, Chengdu University of Technology, Chengdu 610059, China

15 <sup>f</sup> International Center for Sedimentary Geochemistry and Biogeochemistry Research, Chengdu  
16 University of Technology, Chengdu 610059, China

17 <sup>g</sup> School of Earth and Environment, University of Leeds, Leeds LS2 9JT, UK

18 <sup>h</sup> Department of Earth and Planetary Sciences, University of California, Riverside, CA 92521,  
19 USA  
20

21 \* Corresponding author: Lei Zhang, email: [zhanglei\\_cug@sina.com](mailto:zhanglei_cug@sina.com)  
22

23 **Abstract**

24 The Steptoean Positive Carbon Isotope Excursion (SPICE) event at ~497-494 Ma was a  
25 major carbon-cycle perturbation of the late Cambrian that coincided with rapid diversity changes  
26 among trilobites. Several scenarios (e.g., climatic/oceanic cooling, and seawater anoxia) have been  
27 proposed to account for an extinction of trilobites at the onset of SPICE, but the exact mechanism  
28 remains unclear. Here, we present a chemostratigraphic study of carbonate carbon and  
29 carbonate-associated sulfate sulfur isotopes ( $\delta^{13}\text{C}_{\text{carb}}$  and  $\delta^{34}\text{S}_{\text{CAS}}$ ) and elemental redox proxies  
30 ( $U_{\text{EF}}$ ,  $Mo_{\text{EF}}$ , and  $C_{\text{org/P}}$ ), augmented by secular trilobite diversity data, from both upper slope  
31 (Wangcun) and lower slope (Duibian) successions from the Jiangnan Slope, South China,  
32 spanning the Drumian to lower Jiangshanian. Redox data indicate locally/regionally  
33 well-oxygenated conditions throughout the SPICE event in both study sections except for  
34 low-oxygen (hypoxic) conditions within the rising limb of the SPICE (early-middle Paibian) at  
35 Duibian. As in coeval sections globally, the reported  $\delta^{13}\text{C}_{\text{carb}}$  and  $\delta^{34}\text{S}_{\text{CAS}}$  profiles exhibit  
36 first-order coupling throughout the SPICE event, reflecting co-burial of organic matter and pyrite  
37 controlled by globally integrated marine productivity, organic preservation rates and shelf hypoxia.

38 Increasing  $\delta^{34}\text{S}_{\text{CAS}}$  in the 'Early SPICE' interval (late Guzhangian) suggests that significant  
39 environmental change (e.g., global-oceanic hypoxia) was underway before the global carbon cycle  
40 was markedly affected. Assessment of trilobite range data within a high-resolution biostratigraphic  
41 framework for the middle-late Cambrian facilitated re-evaluation of the relationship of the SPICE  
42 to contemporaneous biodiversity changes. Trilobite diversity in South China declined during the  
43 Early SPICE (corresponding to the End-Marjuman Biomere Extinction, or EMBE, of Laurentia)  
44 and at the termination of the SPICE (corresponding to the End-Steptoean Biomere Extinction, or  
45 ESBE, of Laurentia), consistent with biotic patterns from other cratons. We infer that oxygen  
46 minimum zone (OMZ) and/or shelf hypoxia expanded as a result of locally enhanced productivity  
47 due to intensified upwelling following climatic cooling, and that expanded hypoxia played a major  
48 role in the EMBE at the onset of SPICE. During the SPICE event, global-ocean ventilation  
49 promoted marine biotic recovery, but termination of SPICE-related cooling in the late Paibian may  
50 have reduced global-ocean circulation, triggering further redox changes that precipitated the ESBE.  
51 Major changes in both marine environmental conditions and trilobite diversity during the late  
52 Guzhangian demonstrate that the SPICE event began earlier than the Guzhangian-Paibian  
53 boundary, as previously proposed.

54

55 *Keywords:* carbon isotopes; sulfur isotopes; oceanic anoxia; species diversity; Marjuman Biomere;  
56 Steptoean Biomere

57

## 58 **1. Introduction**

59 The Cambrian, a key period in Earth history, was characterized by the Cambrian Explosion of  
60 marine invertebrate life (Marshall, 2006) as well as unstable marine environments as revealed by  
61 fluctuations in carbon isotopes (Saltzman and Thomas, 2012), multiple biotic extinctions, and the  
62 development of extreme environmental conditions (Servais et al., 2010). The Steptoean Positive  
63 Carbon Isotope Excursion (SPICE) was the last major carbon isotope excursion (CIE) of the  
64 Cambrian (Saltzman et al., 1998, 2000), recording a shift of ~4 to 6‰ in marine carbonate carbon  
65 isotopes ( $\delta^{13}\text{C}_{\text{carb}}$ ) for an interval of  $3.0 \pm 0.2$  Myr during the Paibian Stage (~497–494 Ma;  
66 lowermost Furongian Series; Sørensen et al., 2020; see Supplemental Section I for Cambrian  
67 timescale). The SPICE event began at the base of the Paibian Stage, as defined by the first  
68 appearance datum (FAD) of the trilobite *Glyptagnostus reticulatus* (Peng and Robison, 2000; Zhu  
69 et al., 2018), and continued to the base of the *Irvingella major* Zone in the early Jiangshanian  
70 (Peng et al., 2004, 2012; Gerhardt and Gill, 2016), thus spanning from the middle Cambrian  
71 (Miaolingian, formerly Series 3) to the late Cambrian (Furongian) series boundary interval.

72 The SPICE event was associated with a pronounced marine biotic turnover, including  
73 extinctions of trilobites and agnostid arthropods (Palmer, 1984; Saltzman et al., 2000; Gerhardt  
74 and Gill, 2016; Moysiuk and Caron, 2019; Zhang et al., 2021) and brachiopods (Rowell and Brady  
75 1976; Rieboldt, 2005), changes in the composition of reef communities (Lee et al., 2015), and  
76 large increases in plankton diversity (Servais et al., 2008). Middle and upper Cambrian trilobites

77 have been especially well studied, and the SPICE event was accompanied by extinctions of the  
78 Marjumiid Biomere at the end of the Guzhangian Stage and the Pterocephaliid Biomere in the  
79 early Jiangshanian Stage (Palmer, 1979, 1984; Gerhardt and Gill, 2016; Zhang et al., 2021).  
80 Several mechanisms have been proposed to explain the extinction of the Marjumiid Biomere,  
81 including global temperature changes (Lochman-Balk, 1970; Öpik, 1966), a rise in the  
82 thermocline and shelf cooling (Stitt, 1975), and/or ecospace changes linked to sea-level  
83 fluctuations (Ludvigsen, 1982; Westrop, 1988; Westrop and Ludvigsen, 1987). Geochemical  
84 studies have confirmed some of these inferences and proposed other potential causes, for example,  
85 upwelling of cool deep waters onto shallow shelves (Perfetta et al., 1999; Elrick et al., 2011) as  
86 well as widespread oceanic anoxia (Saltzman et al., 1998; Hurtgen et al., 2009; Gill et al., 2011;  
87 2021; Dahl et al., 2014). However, these studies are based on geographically limited datasets  
88 containing a small number of proxies, rendering the causes of the extinction uncertain.

89 Middle-Late Cambrian trilobite extinctions were almost certainly linked to marine  
90 environmental changes, but the nature of such changes during the SPICE event remains poorly  
91 known. The SPICE is thought to have coincided with a major phase of global cooling, although  
92 this inference is based largely on carbon-cycle changes and physical evidence of sea-level fall  
93 rather than direct temperature measurements. In addition to a positive CIE, changes in the global  
94 carbon cycle are indicated by evidence of enhanced marine productivity and organic carbon burial  
95 from organic carbon-nitrogen isotopes (Hammer and Svensen, 2017), carbon-sulfur isotope  
96 modeling of atmospheric O<sub>2</sub> content (Saltzman et al., 2011; Krause et al., 2018), N/P ratios  
97 indicating P limitation of marine productivity (Saltzman, 2005), and a decrease in seawater  
98 <sup>87</sup>Sr/<sup>86</sup>Sr values (Zhang et al., 2020). Physical evidence of cooling includes a sea-level lowstand at  
99 the Sauk-II/III contact (= mid-Paibian) (Saltzman et al., 2000, 2004; Sørensen et al. 2020),  
100 ice-erosional features at mid-latitudes of Baltica (Dronov and Popov 2004; Cherns and Wheeley,  
101 2009), consistent with growth of continental icesheets during the early to middle Paibian  
102 (Matthews and Al-Husseini, 2010; Al-Husseini, 2017). Due to the indirect nature of this evidence,  
103 climate cooling during the early to middle Paibian remains contentious. The only oxygen isotope  
104 (δ<sup>18</sup>O) study of the Paibian to date documented increased sea-surface temperatures on the western  
105 margin and cratonic interior of Laurentia (Elrick et al., 2011; Wotte et al., 2019). However, this  
106 warming event is likely to have been a local signal related to shallowing on a tropical continental  
107 shelf, with glacio-eustatic fall causing the study sections to shallow into the ocean-surface layer,  
108 thus recording locally warmer conditions despite the general climatic cooling necessary to induce  
109 glacial expansion.

110 In the present study, our goals are to examine chemostratigraphic records of marine  
111 paleoenvironmental change during the SPICE, and to link these changes to contemporaneous  
112 records of trilobite diversity in order to better understand controls on Middle-Late Cambrian biotic  
113 events. We analyzed two middle to upper Cambrian sections in South China, Wangcun and  
114 Duibian, representing relatively shallower (upper slope) and deeper (lower slope) depositional  
115 settings, applying elemental redox proxies (i.e., U<sub>EF</sub>, Mo<sub>EF</sub>, C<sub>org</sub>/P) to track local environmental

116 changes that may have affected biodiversity patterns, and inorganic carbon and sulfur isotopes (i.e.,  
117  $\delta^{13}\text{C}_{\text{carb}}$  and  $\delta^{34}\text{S}_{\text{CAS}}$ ; carb = carbonate; CAS = carbonate-associated sulfate) as global seawater  
118 proxies. Furthermore, we reprocessed published trilobite data for these two sections, which are  
119 among the faunally best studied successions of middle to late Cambrian age globally, having  
120 yielded a wealth of trilobite taxonomic data suitable for analysis of biodiversity trends. Our study  
121 thus provides an integrated geochemical and paleontological dataset that addresses fundamental  
122 relationships between paleoenvironmental changes and biotic evolution during the SPICE event.

123

## 124 **2. Geological background**

### 125 *2.1. Paleogeography*

126 During the middle and late Cambrian, the South China Craton was located on the equatorial  
127 margin of Gondwana (Fig. 1A). Three main depositional environments existed along a  
128 platform-to-basin transect, with a shallow-platform carbonate facies to the northwest (Yangtze  
129 Platform), argillaceous carbonate and shale in the central slope facies (Jiangnan Slope), and  
130 fine-grained siliciclastic and chert in the basinal facies (Nanhua Basin) to the southeast (Fig. 1B;  
131 Feng et al., 2002; note: all coordinates are modern unless otherwise noted). The present study  
132 sections are located on the Jiangnan Slope (Zuo, et al., 2018).

133

### 134 *2.2. Wangcun section*

135 Wangcun (GPS: 28°43'2.84" N, 109°58'26.10" E) is an outcrop section exposed along a  
136 roadcut on the northern bank of the Youshui River in western Hunan Province, South China (Fig.  
137 1C). It is a parastratotype of the Drumian-Guzhangian stage boundary, for which the Global  
138 Stratotype Section and Point (GSSP) is the Luoyixi section, which is located on the southern bank  
139 of the same river (Peng et al., 2004, 2005, 2009). The Wangcun section consists, in ascending  
140 order, of the Aoxi, Huaqiao, and Shenjiawan formations. The Aoxi Formation is mainly composed  
141 of dolomite and black shale interbedded with limestone; the Huaqiao Formation is dominated by  
142 thin-bedded muddy limestone, with a few oolitic limestone beds in the lower part, and  
143 thick-bedded mudstone containing lenticular limestone, conglomeratic limestone, and calcareous  
144 shale beds in the upper part; and the Shenjiawan Formation consists of limestone and dolomitic  
145 limestone (Peng et al., 2004; Fig. 2).

146 The trilobite biostratigraphy of the Wangcun section is well studied for the Drumian and  
147 Guzhangian stages, but less so for the Paibian and Jiangshanian stages (Fig. 2A). A total of 9  
148 trilobite zones have been established, in ascending order, the *Ptychagnostus atavus*, *Pt.*  
149 *punctuosus*, *Goniagnostus nathorsti*, *Lejopyge armata*, *L. laevigata*, *Proagnostus bulbus*,  
150 *Linguagnostus reconditum*, *Glyptagnostus stolidotus*, and *G. reticulatus* zones. The bases of the  
151 Drumian, Guzhangian, and Paibian stages are defined by the first appearance datums (FADs) of  
152 the trilobites *P. atavus*, *L. laevigata*, and *G. reticulatus*, respectively (Peng, 2005; Peng et al.,  
153 2009). The placement of the top of the *G. reticulatus* Zone and the stratigraphic interval of the *Ag.*  
154 *orientalis* Zone (note: the base of this zone is equivalent to the base of the Jiangshanian) are

155 defined based on correlations with Duibian A (Zuo et al., 2018).

156

### 157 2.3. Duibian section

158 The Duibian section consists of outcrops near Duibian village, 10 km north of Jiangshan City,  
159 western Zhejiang Province, South China (Fig. 1D). Duibian A (GPS: 28°48'48.38" N, 118°37'19.21"  
160 E), a parastratotype of the Paibian-Jiangshanian stage boundary, contains, in ascending order, the  
161 upper Yangliugang, Huayansi, and lower Siyanshan formations (Lu and Lin, 1989; Peng et al.,  
162 2012). The Yangliugang Formation consists mainly of dark-gray, thin-bedded dolomitic limestone  
163 with calcareous mudstone interbeds; the Huayansi Formation comprises dark, thin-bedded  
164 limestone with thin shale interbeds and light-colored ribbon limestones; and the Siyangshan  
165 Formation consists of pale limestone with breccias in the lower part, and light gray thin-bedded  
166 limestone interbedded with calcareous mudstone and muddy limestone in the upper part. Duibian  
167 B (28°48'46.14" N, 118°37'17.20" E), the GSSP for the Paibian-Jiangshanian stage boundary, is  
168 located ~250 m to the south of Duibian A and exposes only a part of the Huayansi Formation (Fig.  
169 1D). Although their chemostratigraphic profiles are shown separately in the figures of this study,  
170 the geochemical datasets of Duibian A and B were combined for purposes of statistical evaluation  
171 owing to their proximity and general similarity.

172 The trilobite biostratigraphy of the Duibian section (Figs. 3A, 4A) is well established (Lu and  
173 Lin, 1989; Peng et al., 2012). At Duibian A, the bases of the Paibian and Jiangshanian stages are  
174 defined by the FADs of the trilobites *Glyptagnostus reticulatus* and *Agnostotes orientalis*,  
175 respectively. Duibian B is the GSSP of the base of the Jiangshanian Stage, based on the FAD of  
176 the trilobite *Ag. orientalis* (Peng et al., 2012). The base of the Jiangshanian Stage was placed at  
177 116.6 m and 108.12 m above the base of the Huayansi Formation at Duibian A and B, respectively  
178 (Peng et al., 2012).

179

### 180 2.4. Comparative global sections

181 Results from the study sections were compared with geochemical data from five widely  
182 distributed SPICE sections (Fig. 1A). Four of these auxiliary sections accumulated on continental  
183 shelves, ranging from subtidal-peritidal to deep-shelf settings: (1) Lawson Cove, Utah (Gill et al.,  
184 2011; note: not "Lawsons Cove" as given in that source); (2) Shingle Pass, Nevada (Saltzman et  
185 al., 1998; Gill et al., 2007); (3) Mount Whelan core, Australia (Saltzman et al., 2000; Gill et al.,  
186 2011); and (4) TE-1 core, Texas County, Missouri (Gill et al., 2011). The fifth auxiliary section,  
187 the Andrarum-3 core (Sweden), was deposited below storm wave base (Gill et al., 2011; Dahl et  
188 al., 2013). Paired  $\delta^{13}\text{C}_{\text{carb}}$  and  $\delta^{34}\text{S}_{\text{CAS}}$  values for the five auxiliary sections, as well as local/global  
189 redox proxy data for two of the five sections (i.e., carbonate uranium isotopes from Mount Whelan  
190 core, and redox sensitive elements from Andrarum-3 core) were available for comparisons (note:  
191 the other three auxiliary sections lack such data). See Supplemental Section 2 and Table S1 for  
192 more paleogeographic and stratigraphic background information about the study and auxiliary  
193 sections, and Supplemental Figure S1 for correlation of trilobite zones between South China and

194 Laurentia.

195

### 196 2.5. Internal stratigraphy of the SPICE event interval

197 Previous studies have divided the SPICE interval into two parts: a ‘rising limb’ marked by an  
198 increasing trend of carbonate carbon isotopes ( $\delta^{13}\text{C}_{\text{carb}}$ ), and a ‘falling limb’ marked by a  
199 decreasing  $\delta^{13}\text{C}_{\text{carb}}$  trend (Saltzman et al., 2000; Pulsipher et al., 2021). In the present study, we  
200 identify a third interval that we term ‘Early SPICE’, marking the earliest stage of the SPICE event  
201 prior to a major rise in  $\delta^{13}\text{C}_{\text{carb}}$ . In addition, for the sake of ease of reference, we term the intervals  
202 that preceded and followed the SPICE event the ‘Pre-SPICE’ and ‘Post-SPICE’, respectively. In  
203 our study sections, the Pre-SPICE, Early SPICE, Rising SPICE (= ‘rising limb’), Falling SPICE (=‘  
204 falling limb’), and Post-SPICE intervals correspond to Units I to V (in sequence). For sections  
205 having a substantial Pre-SPICE interval, we have designated the somewhat older carbon isotope  
206 excursion known as DICE (Drumian Carbon Isotope Excursion) as Unit Ia and the strata between  
207 DICE and the base of the Early SPICE as Unit Ib. All five units are present at Wangcun (Fig. 2C),  
208 but only four units (Ib, II, III and IV) are present at Duibian A (Fig. 3C), and only two units (IV  
209 and V) at Duibian B (Fig. 4C).

210 The five intervals described above were defined primarily on the basis of carbonate carbon  
211 isotope ( $\delta^{13}\text{C}_{\text{carb}}$ ) variation (cf. Saltzman et al., 2000; Pulsipher et al., 2021) but with reference to  
212 some secondary criteria including the  $\delta^{34}\text{S}_{\text{CAS}}$  profile and trilobite range data. To facilitate use in  
213 other studies, we define the subdivisions primarily in terms of carbon isotope variation and  
214 trilobite range data. The Early SPICE interval is marked by a gentle rise of  $\delta^{13}\text{C}$  (note: not the  
215 steep rise associated with the Rising SPICE), or, in sections lacking such a  $\delta^{13}\text{C}$  feature, by a  
216 significant rise of  $\delta^{34}\text{S}_{\text{CAS}}$ , during the late to latest Guzhangian Stage (*Linguagnostus reconditus*  
217 and *G. stolidotus* zones). The transition from the Early SPICE to Rising SPICE is marked by a  
218 sharp acceleration in the  $\delta^{13}\text{C}$  profile, or by the onset of rising  $\delta^{13}\text{C}$  in sections lacking the slow  
219  $\delta^{13}\text{C}$  rise of the Early SPICE; it spans the earliest Paibian (base of *G. reticulatus* Zone) to middle  
220 Paibian Stage (*A. inexpectans* Zone). The transition from the Rising SPICE to Falling SPICE is  
221 marked by the shift from increasing to decreasing  $\delta^{13}\text{C}$  values; in some sections (e.g., Shingle Pass,  
222 Lawson Cove, TE-1 Texas County Core, Mount Whelan Core; Saltzman et al., 1998, 2000; Gill et  
223 al., 2007, 2011) this transition is rapid, but in other sections (e.g., Deogwoo, Wa’ergang, House  
224 Range; Baker, 2010; Chung et al., 2011; Li et al., 2018) there is an extended plateau of nearly  
225 uniform high  $\delta^{13}\text{C}$  values that makes identification of the exact point of the transition somewhat  
226 arbitrary. The Falling SPICE corresponds to the middle Paibian to early Jiangshanian Stage (i.e., *A.*  
227 *inexpectans* Zone to lower part of *Ag. orientalis* Zone). The Pre-SPICE and Post-SPICE are  
228 defined simply as those intervals preceding onset of the Early SPICE and following termination of  
229 the Falling SPICE, respectively. The Post-SPICE corresponds to middle-late Jiangshanian Stage  
230 (i.e., upper part of *Ag. orientalis* Zone to *Eolotagnostus* Zone).

231 Our scheme for internal subdivision of the SPICE event redefines the timing of its onset.  
232 Earlier studies placed the base of the SPICE event at the onset of the sharp rise in the  $\delta^{13}\text{C}_{\text{carb}}$

233 profile (e.g., Saltzman et al., 2000; Zhu et al., 2018; Pulsipher et al., 2021; but note that  
234 Schiffbauer et al., 2017 proposed a globally diachronous onset of the SPICE), which is equivalent  
235 to the base of the Rising SPICE of our study. However, the present study demonstrates that the  
236 former definition is inconvenient for three reasons. First, the Wangcun and Duibian sections show  
237 positive shifts in  $\delta^{13}\text{C}_{\text{carb}}$  and  $\delta^{34}\text{S}_{\text{CAS}}$  heralding the SPICE event well below the  
238 Guzhangian-Paibian boundary, which has previously defined the base of the SPICE (Saltzman et  
239 al., 2000). At Wangcun, obvious positive shifts commence at ~210 m, or ~70 m below the base of  
240 the Rising SPICE (which is at ~280 m), and at Duibian A, obvious positive shifts commence at  
241 ~4 m, or ~11 m below the base of the Rising SPICE (which is at ~7 m; Figs. 2-3). Second, the  
242 concurrent positive shifts of  $\delta^{13}\text{C}_{\text{carb}}$  and  $\delta^{34}\text{S}_{\text{CAS}}$  during the late Guzhangian Stage were a global  
243 phenomenon (Gill et al., 2007; Pulsipher et al., 2021), and they coincided with the initiation of  
244 shifts in other global proxies (e.g.,  $\delta^{238}\text{U}$  values) that continued into the Rising SPICE interval  
245 (Dahl et al., 2014). Third, the former definition decouples the SPICE from the EMBE, leading to  
246 suggestions that the EMBE had non-SPICE-related causes (Palmer, 1984; Saltzman et al., 2000;  
247 Elrick et al., 2011), which we regard as almost certainly incorrect. For these reasons, we propose  
248 redefinition of the base of the SPICE based on the onset of paleo-environmental disturbances as  
249 determined from multiple proxies (i.e.,  $\delta^{13}\text{C}_{\text{carb}}$ ,  $\delta^{34}\text{S}_{\text{CAS}}$ ,  $\delta^{98}\text{Mo}$  and  $\delta^{238}\text{U}$ ), instead of a single  
250 proxy ( $\delta^{13}\text{C}_{\text{carb}}$ ) that exhibits invariant or regionally variable values during the EMBE (e.g.,  
251 Gerhardt and Gill, 2016; Schiffbauer et al., 2017). The interval of slowly rising  $\delta^{13}\text{C}_{\text{carb}}$  during the  
252 earliest part of the redefined SPICE is herein termed the “Early SPICE” interval (Unit II of present  
253 study, within the *Li. reconditus* and *G. stolidotus* zones) (Figs. 2-3). This redefinition places the  
254 onset of the SPICE event in the late Guzhangian rather than at the Guzhangian-Paibian stage  
255 boundary (cf. Saltzman et al., 2000), and it links middle-late Cambrian trilobite diversity changes  
256 more effectively to the trajectory of the SPICE event (cf. Gerhardt and Gill, 2016; Zhang et al.,  
257 2021).

258

### 259 3. Methods

#### 260 3.1. Isotopic and elemental analyses

261 Weathered surfaces and diagenetic veins were trimmed off, and the remaining bulk-rock  
262 carbonate was powdered to <74  $\mu\text{m}$  (200 mesh) using a rock mill. Major elements were measured  
263 using wavelength-dispersive XRF and trace elements using ICP-MS, after sample powder  
264 digestion by  $\text{HNO}_3$  and HF, in the State Key Laboratory of Geological Processes and Mineral  
265 Resources at the China University of Geosciences–Wuhan. Average analytical uncertainty is  
266 better than 5% (RSD) for major elements based on repeated analysis of national standards  
267 GBW07132, GBW07133 and GBW07407, and better than 2% (RSD) for trace elements based on  
268 international standards AGV-2, BHVO-2, BCR-2 and GSR-1. In the same laboratory, total organic  
269 carbon (TOC) content was measured using an Elementar Vario Micro Cube Analyzer, and  
270 inorganic carbon isotopes were measured using a 253 Plus Isotope Ratio Mass Spectrometer  
271 (IR-MS) interfaced with a Kiel IV auto-sampler. The analytical precision was better than 0.04%

272 for both  $\delta^{13}\text{C}_{\text{carb}}$  and  $\delta^{18}\text{O}_{\text{carb}}$  based on duplicate analyses of national standards GBW-04416 and  
273 GBW-04417. Multiple NaCl rinses (generally > 30 times) was applied to extract  
274 carbonate-associated sulfate (CAS) (Wotte et al., 2012). Sulfur isotopes in CAS were analyzed  
275 using a Delta V plus IR-MS in the State Key Laboratory of Biogeology and Environmental  
276 Geology at the China University of Geosciences–Wuhan. Analytical errors were 0.08 ‰, 0.09 ‰  
277 and 0.20 ‰ (1 $\sigma$ ), respectively, calculated from duplicate analyses of the international standards  
278 NBS 127, IAEA SO-5, and IAEA SO-6. Detailed descriptions of all methods are given in  
279 Supplemental Section 3.

280

### 281 3.2. *Trilobite biodiversity*

282 Trilobite biostratigraphic analyses at Wangcun were carried out by Peng and Robison (2000)  
283 and Peng et al. (2009), during investigation of the nearby Luoyixi section as the GSSP of the base  
284 of the Guzhangian Stage. A total of 66 species (including 2 undefined species) were recognized  
285 from ~90 stratal levels at Wangcun, including within the Pre-SPICE and Early SPICE intervals  
286 (~150- and ~100-m-thick, respectively), and the lower part of the Rising SPICE (20-m-thick).

287 Trilobite biostratigraphic work at Duibian was carried out by Lu and Lin (1989) and Peng et  
288 al. (2006, 2009, 2012) before designation of this locale as the GSSP of the base of the  
289 Jiangshanian Stage. A total of 64 species (including 14 undefined species) were recognized from  
290 ~50 stratal levels within a ~200-m-thick interval containing the SPICE event at Duibian A, and 35  
291 species (including 9 undefined species) from ~30 stratal levels within a ~40-m-thick interval at  
292 Duibian B.

293 In the present study, we compiled trilobite species range data in order to construct both  
294 species diversity and range-through diversity profiles for each study section for the lowermost  
295 Drumian to lower Jiangshanian interval. The *species diversity curve* shows the total number of  
296 trilobite species actually identified at a given stratal level in the source studies (Peng and Robison,  
297 2000; Peng et al., 2004, 2005, 2006, 2009, 2012). The *range-through diversity curve* accounts for  
298 taxa that are absent at a given stratigraphic level but present in both underlying and overlying  
299 horizons, on the assumption that their absence in such cases is due to incompleteness of the fossil  
300 record.

301

## 302 4. Results

### 303 4.1. *Variations of isotopic and elemental proxies*

304 The  $\delta^{13}\text{C}_{\text{carb}}$  profiles of the study sections exhibit a broad first-order positive excursion  
305 representing the SPICE, spanning a stratigraphic interval of 229.0 m to 361.0 m at Wangcun and  
306 -4.0 m to 29.0 m at Duibian A-B (Figs. 2-4). From background values of ~-0.1 ‰ (Unit Ib;  
307 Pre-SPICE), the excursion began in the late Guzhangian with a slow initial shift that was slightly  
308 larger at Wangcun (~+1 ‰) relative to Duibian A (~+0.5 ‰) (Unit II; Early SPICE). A steeper rise  
309 in  $\delta^{13}\text{C}_{\text{carb}}$  commenced at the Guzhangian-Paibian boundary, marking the onset of the main phase  
310 of SPICE (Unit III; Rising SPICE). The positive excursion peaked in the middle Paibian with

311 values of +3.84 ‰ at Wangcun and +3.15 ‰ at Duibian A.  $\delta^{13}\text{C}_{\text{carb}}$  values declined during the late  
312 Paibian to early Jiangshanian (Unit IV; Falling SPICE), stabilizing at ~1 ‰ in the Post-SPICE  
313 interval (Unit V). The full SPICE excursion appears relatively smoother at Wangcun than at  
314 Duibian, where some small-scale variability is present (e.g., in Unit III), although this difference  
315 may be due to the higher-resolution sampling of the latter section.

316 The  $\delta^{34}\text{S}_{\text{CAS}}$  profiles of the study sections also show first-order positive excursions during the  
317 SPICE (Figs. 2-4). Following background values of ~25-35 ‰ in the Pre-SPICE, a major rise of  
318  $\delta^{34}\text{S}_{\text{CAS}}$  begins in the Early SPICE, reaching a peak value that is slightly higher at Wangcun  
319 (+48.4 ‰) relative to Duibian A (+46.9 ‰). Relatively stable plateau values are observed at  
320 Wangcun (~+40-50 ‰) and Duibian A (~+35-45 ‰) in the Rising SPICE, but  $\delta^{34}\text{S}_{\text{CAS}}$  shows a  
321 decreasing trend to a minimum of ~+28 ‰ (Wangcun) and ~+20-25 ‰ (Duibian) by the end of  
322 the Falling SPICE.  $\delta^{34}\text{S}_{\text{CAS}}$  fluctuates within ~5-25 ‰ and finally maintains stable values  
323 (~25-30 ‰) in the Post-SPICE at Wangcun, with a comparable range of fluctuations (within  
324 ~15-35 ‰) at Duibian B.

325 The TOC profile at Wangcun shows a roughly decreasing trend from ~0.6 to ~0.2 wt.% with  
326 a few peak values (to ~0.6-1.0 wt.%) in the DICE to Early SPICE intervals, then maintains  
327 relatively low values (~0.2 wt.%) punctuated by several sharp peaks (to ~0.6-1.4 wt.%) in the  
328 Rising to Post-SPICE intervals (Fig. 5B). The TOC profiles show more regular variations at  
329 Duibian, stabilizing around 0.10 wt.% in the Pre-SPICE, rising to relatively higher level (~0.2  
330 wt.%) with few peak values (~0.5-2.0 wt.%) in the Rising SPICE, then gradually dropping in the  
331 Falling SPICE and reaching a minimum of ~0.02 wt.% by its termination, before sharply rising to  
332 a peak value ~0.4 wt.% and fluctuating over ~0.1-0.8 wt.% in the Post-SPICE (Fig. 6B, 7B).

333 The  $C_{\text{org}}/P$  profile at Wangcun exhibits low values (mostly < 5) in the DICE and Early SPICE,  
334 then rises to relatively higher values of ~60-80 in the Early and Rising SPICE, followed by a  
335 return to lower values of ~0-50 in the Falling SPICE, before fluctuating in the range of ~0-100 in  
336 the Post-SPICE (Fig. 5F). At Duibian, relative to background values (~0-20) in the Pre-SPICE,  
337  $C_{\text{org}}/P$  rises progressively to ~30 in the Early SPICE, then remains at a plateau (~25-45)  
338 punctuated by several peaks (to ~50-200) in the Rising SPICE, before gradually dropping to  
339 minimum values (< 5) in the Falling SPICE, and finally rebounding to relatively higher values  
340 (~15-45) in the Post-SPICE (Fig. 6F, 7F).

341 Trace-element enrichment factors (EFs) were calculated as  $X_{\text{EF}} = (X/\text{Al})_{\text{sample}} / (X/\text{Al})_{\text{UCC}}$ ,  
342 where UCC is average upper crustal composition (McLennan, 2001). In order to reduce variance  
343 in EFs related to small denominator values, only samples with Al > 0.5% were used in redox  
344 reconstructions (Figs. 5-7; see also Supplemental Fig. S3). At Wangcun, the  $U_{\text{EF}}$  and  $Mo_{\text{EF}}$   
345 profiles exhibit decreasing trends from ~15 to ~3 and ~64 to ~1, respectively, in the DICE to  
346 Pre-SPICE intervals, and then both profiles exhibit lower values (mostly < 3) in the Early SPICE  
347 to Post-SPICE (Fig. 5D-E). At Duibian A, the  $U_{\text{EF}}$  profile shows a decreasing trend (~7 to ~2) in  
348 the Pre-SPICE to Early SPICE, followed by stable values (~3-5) in the Rising SPICE, before  
349 increasing (to >10) in the Falling SPICE (Fig. 6D). The  $Mo_{\text{EF}}$  profile mostly exhibits low values

350 ( $\sim < 3$ ) in the Pre-SPICE to Early SPICE, then rises to slightly higher values ( $\sim 3$  to  $\sim 9$ ) in the  
351 Rising SPICE, before dropping to a minimum ( $\sim 1$ ) in the Falling SPICE (Fig. 6E). At Duibian B,  
352  $U_{EF}$  fluctuates between  $\sim 2$  and  $\sim 17$ , and  $Mo_{EF}$  between  $\sim 1$  and  $\sim 10$ , in the Falling SPICE to  
353 Post-SPICE interval (Fig. 7D-E).

354

#### 355 4.2. Trilobite species diversity records

356 At Wangcun, trilobite range-through species diversity rises from 2 to 9 at  $\sim 30$ -80 m (i.e.,  
357 within the *Ptychagnostus aculeatus* Zone), remains stable ( $\sim 5$ ) at  $\sim 80$ -150 m (i.e., lower part of  
358 the Pre-SPICE), followed by a slight increase to  $\sim 10$ -15 at  $\sim 220$  m (i.e., upper part of the  
359 Pre-SPICE), before a significant decrease to a minimum of 1 at  $\sim 270$  m (base of the *G. stolidotus*  
360 Zone, i.e., the EMBE), and with the minimum value continuous into the Rising SPICE (base of the  
361 *G. reticulatus* Zone) (Fig. 2).

362 At Duibian A, trilobite range-through species diversity rises significantly from  $< 10$  at the  
363 base of the section (lower Guzhangian) to a maximum value of 25 at  $-5$  m prior to the onset of the  
364 Early SPICE (base of the *Li. reconditus* Zone) (Fig. 3). Between  $-5$  m and 0 m (base of the *G.*  
365 *stolidotus* Zone, i.e., EMBE), range-through species diversity drops sharply to  $< 5$ , followed by a  
366 gradual decline to 0 at 30 m, representing the end of the Rising SPICE (lower part of the *A.*  
367 *inexpectans* Zone). Upwards, range-through species diversity gradually rises to  $\sim 5$ -10 at 70 m  
368 (end of Falling SPICE) before a decline to  $< 5$  at the top of the section (within the *Ag. orientalis*  
369 Zone, i.e., ESBE). At Duibian B, trilobite range-through species diversity gradually increases from  
370 0-5 at the base of the section to a maximum of 15 at 28 m (end of the Falling SPICE; upper part of  
371 the *A. inexpectans* Zone), followed by a decrease to  $< 5$  at 35-40 m (i.e., ESBE) within the  
372 Post-SPICE interval at the top of the section (middle part of the *Eolotagnostus* Zone) (Fig. 4).

373

## 374 5. Discussion

### 375 5.1. Data evaluation

#### 376 5.1.1. CAS extraction methods

377 The extraction method of CAS (i.e., using multiple NaCl rinses) that we applied in the  
378 present study is likely to remove a large part of the contaminant secondary sulfate, for example,  
379 that from soluble and organically bound sulfur as well as diagenetically oxidized pyrite. Repeated  
380 leaching with an NaCl solution is recommended as a standard step in CAS extraction from  
381 carbonate rocks, as it can fully remove non-CAS sulfate that was not incorporated into the  
382 carbonate mineral structure. It is superior to using NaOCl or  $H_2O_2$  rinses alone, or a combination  
383 thereof with NaCl rinses (Wotte et al., 2012). We generally repeated NaCl rinses at least 30 times,  
384 which is more effective than a small number of NaCl rinses or a single NaCl rinse followed by an  
385 NaOCl rinse (Edwards et al., 2019), as the latter two methods are unlikely to fully remove  
386 non-CAS sulfate. Although [CAS] is low in Duibian samples ( $\sim 1$ -4 ppm), making  $\delta^{34}S_{CAS}$   
387 susceptible to the influence of oxidized pyrite prior to or during laboratory pretreatment, we infer  
388 that such effects were probably minor because the  $\delta^{34}S_{CAS}$  profiles of the study sections exhibit

389 relatively high values (mostly > 20 ‰) relative to those of pyrite sulfur (< ~-10 ‰) as well as  
390 stable stratigraphic trends without anomalous negative outliers.

391

### 392 5.1.2. *Effects from local depositional conditions and early marine diagenesis*

393 Local depositional conditions and early marine diagenesis determine preservation of marine  
394 carbonate and regional/global stratigraphic expressions of carbon-isotopic signals in shallow-water  
395 carbonate facies. Large glacio-eustatic fluctuations can result in isotopic shifts unrelated to  
396 variations in the global carbon cycle (Swart, 2008, 2015; Swart and Kennedy, 2012). For example,  
397 flooding of carbonate platforms can increase the proportion of aragonite in sediments, resulting in  
398 a globally synchronous positive  $\delta^{13}\text{C}$  excursion. Conversely, sea-level fall results in exposure of  
399 platform carbonates to freshwater, leading to meteoric diagenetic alteration in which enhanced  
400 authigenic carbonate precipitation can generate a negative  $\delta^{13}\text{C}$  excursion (Schrag et al., 2013;  
401 Zhao et al., 2016). However, the positive  $\delta^{13}\text{C}_{\text{carb}}$  excursion of the SPICE event was associated  
402 with a major sea-level fall (e.g., Saltzman et al., 2000), arguing against the influence of sea-level  
403 variation on marine carbonate carbon-isotopic compositions. Previous studies have inferred that  
404 the SPICE was facies-dependent, through intrusion of  $^{13}\text{C}$ -enriched deepwaters onto carbonate  
405 platforms during sea-level rise (Schiffbauer et al., 2017). However, the recognition of the Early  
406 SPICE interval in the present study suggests that the influence of facies on carbon-isotopic  
407 compositions was weak. In addition, regional anoxia-euxinia generally corresponds to positive  
408  $\delta^{13}\text{C}_{\text{carb}}$  excursions during the SPICE (e.g., Gill et al., 2011), indicating that the influence of  
409 authigenic carbonates was limited.

410 Local depositional conditions and early marine diagenesis determine the preservation of  
411 primary  $\delta^{34}\text{S}_{\text{CAS}}$  signals (Present et al., 2019; Richardson et al., 2019, 2021). Generally, low and  
412 stable  $\delta^{34}\text{S}_{\text{CAS}}$  values are associated with deep-water facies, whereas higher and more variable  
413 values characterize shallow-water facies (Richardson et al., 2019). For example, carbonate rocks  
414 deposited in slope facies may incorporate sulfate from anoxic marine-phreatic pore fluids that  
415 have been isotopically modified from seawater by microbial sulfate reduction (Present et al.,  
416 2019). In the present study, Wangcun and Duibian are located in slope areas in which oxic-suboxic  
417 conditions prevailed (see Section 5.2.1), suggesting that the influence of facies on  $\delta^{34}\text{S}_{\text{CAS}}$  signals  
418 was limited. However, facies-related influences on  $\delta^{34}\text{S}_{\text{CAS}}$  signals may have been pronounced in  
419 deep-water SPICE successions such as TE-1 Texas County Core (Gill et al., 2011), which is  
420 characterized by  $\delta^{34}\text{S}_{\text{CAS}}$  that is ~10 to 20 ‰ lower than in shallow-water successions such as the  
421 Mount Whelan Core (see Supplementary Information). Moreover,  $\delta^{34}\text{S}_{\text{CAS}}$  profiles exhibit variable  
422 values in slope sections globally (see Section 5.3), suggesting potential facies or geographic  
423 dependency of primary  $\delta^{34}\text{S}_{\text{CAS}}$  signals during the SPICE event.

424

### 425 5.1.3. *Diagenetic alteration*

426 The present  $\delta^{13}\text{C}_{\text{carb}}$  profiles are interpreted as primary marine signals based on relationships  
427 with  $\delta^{18}\text{O}_{\text{carb}}$  and Mn/Sr ratios (see Supplemental Fig. S2). Generally, Mn/Sr ratios > ~2 and strong

428 covariation with Mn/Sr or  $\delta^{18}\text{O}_{\text{carb}}$  are taken as evidence of diagenetic alteration in carbonate rocks  
429 (Marshall, 1992; Brand, 2004). At Wangcun and Duibian, Mn/Sr ratios are low (avg.  $0.41 \pm 0.33$ ,  
430  $0.1 \pm 0.07$  and  $0.06 \pm 0.06$ , respectively), consistent with little to no diagenetic alteration of the  
431 samples. Moreover,  $\delta^{13}\text{C}_{\text{carb}}$  shows only weak correlation to Mn/Sr ( $r = -0.32$ ,  $n = 37$ ,  $p(\alpha) < 0.05$ ;  
432  $r = -0.39$ ,  $n = 100$ ,  $p(\alpha) < 0.01$ , respectively), and none correlation to  $\delta^{18}\text{O}_{\text{carb}}$  ( $r = -0.13$ ,  $n = 48$ ,  
433  $p(\alpha) > 0.10$ ;  $r = -0.11$ ,  $n = 130$ ,  $p(\alpha) > 0.10$ , respectively).

434 Primary marine  $\delta^{34}\text{S}_{\text{CAS}}$  signals were further evaluated based on relationships to  $\delta^{18}\text{O}_{\text{carb}}$ ,  
435 Mn/Sr, Mg/Ca, and CAS concentrations (see Supplemental Fig. S2). Generally, diagenetic  
436 alteration and dolomitization of carbonate rocks produces strong covariation between  $\delta^{34}\text{S}_{\text{CAS}}$ ,  
437  $\delta^{18}\text{O}_{\text{carb}}$ , Mn/Sr and Mg/Ca (cf. Marengo et al., 2008). However, such effects are not evident at  
438 Wangcun or Duibian, because  $\delta^{34}\text{S}_{\text{CAS}}$  shows weak or no relationship to  $\delta^{18}\text{O}_{\text{carb}}$  ( $r = -0.17$ ,  $n = 34$ ,  
439  $p(\alpha) > 0.10$ ;  $r = -0.24$ ,  $n = 81$ ,  $p(\alpha) < 0.05$ , respectively), Mn/Sr ( $r = -0.45$ ,  $n = 34$ ,  $p(\alpha) < 0.01$ ;  $r$   
440  $= -0.01$ ,  $n = 81$ ,  $p(\alpha) > 0.10$ , respectively) and Mg/Ca ( $r = 0.00$ ,  $n = 34$ ,  $p(\alpha) > 0.10$ ;  $r = -0.34$ ,  $n$   
441  $= 81$ ,  $p(\alpha) < 0.01$ , respectively). Although  $\delta^{34}\text{S}_{\text{CAS}}$  may become coupled to CAS concentrations  
442 through diagenetic, dolomitization or chemical extraction processes (Marengo et al., 2008; Wotte  
443 et al., 2012), the lack of  $\delta^{34}\text{S}_{\text{CAS}}$ -CAS relationships at Wangcun and Duibian ( $r = -0.28$ ,  $n = 34$ ,  
444  $p(\alpha) > 0.10$ ;  $r = -0.19$ ,  $n = 81$ ,  $p(\alpha) \sim 0.05$ , respectively) is consistent with little to no  
445 post-depositional alteration. Additionally,  $\delta^{34}\text{S}_{\text{CAS}}$  variations during the SPICE are similar to those  
446 reported from multiple middle-upper Cambrian sections globally (see Section 5.3). Therefore, the  
447  $\delta^{34}\text{S}_{\text{CAS}}$  profile in the present study is inferred to represent a well-preserved primary marine  
448 isotopic record.

449

## 450 5.2. Oceanic redox conditions during the SPICE

### 451 5.2.1. Redox conditions in study sections

452 Redox changes on the Jiangnan Slope during the SPICE can be evaluated using elemental  
453 proxies (i.e.,  $U_{\text{EF}}$ ,  $Mo_{\text{EF}}$ , and  $C_{\text{org}}/P$ ). Uptake of U commences under suboxic conditions (i.e.,  
454 around the Fe(III)/Fe(II) redox threshold), whereas uptake of Mo requires euxinic conditions (i.e.,  
455 presence of aqueous hydrogen sulfide) (Algeo and Li, 2020). Mo-U enrichment can be used to  
456 roughly assess bottomwater redox conditions, with  $U_{\text{EF}}$  of  $<3$ ,  $\sim 3$ -10, and  $>10$  and  $Mo_{\text{EF}}$  of  $<5$ ,  
457  $\sim 5$ -50, and  $>50$  indicative of oxic, suboxic, and euxinic environments, respectively (Algeo and  
458 Tribouillard, 2009; Scott and Lyons, 2012). However, the threshold values of  $Mo_{\text{EF}}$  and  $U_{\text{EF}}$  are  
459 likely to be formation-specific and may vary between depositional systems due to differing uptake  
460 pathways (Algeo and Liu, 2020).  $C_{\text{org}}/P$  ratios are especially useful for redox assessments in  
461 carbonate facies (in which low organic content can limit trace-metal uptake), with values of  $<50$ ,  
462  $\sim 50$ -100, and  $>100$  indicative of oxic, suboxic, and anoxic environments, respectively (Algeo and  
463 Ingall, 2007). The P in the study units was originally deposited in association with organic matter  
464 and/or Fe-(oxyhydr)oxides rather than carbonate minerals, and it was thus sensitive to redox  
465 changes, as shown by positive correlations with TOC and  $\text{Fe}_2\text{O}_3$ , and negative correlations with  
466 CaO (see Supplemental Fig. S3).

467 In the study sections,  $U_{EF}$  and  $Mo_{EF}$  values are mostly low ( $<10$ ), indicating that oxic to  
468 mildly suboxic conditions prevailed throughout the SPICE event (Figs. 5-7). At Wangcun,  $U_{EF}$  and  
469  $Mo_{EF}$  peaks are found mainly in samples with low Al content, suggesting that they are artifacts of  
470 using a small denominator in the EF calculation. At Duibian A, a shift to moderately reducing (i.e.,  
471 suboxic) conditions during the Rising SPICE (Unit III) is documented by high  $U_{EF}$  (to 5-10)  
472 combined with low  $Mo_{EF}$  ( $\sim 1$ ) for samples with  $Al_2O_3 > 1\%$ , obviating the possibility of an artifact  
473 associated with low Al content. A  $U_{EF}$  vs.  $Mo_{EF}$  crossplot shows that most samples plot in the oxic  
474 field, except for a few close to the suboxic field (Fig. 8A-C).  $C_{org}/P$  ratios are mostly  $<30$ , which  
475 strongly supports oxic conditions, with slightly higher values (to  $\sim 50$ ) only within Unit III,  
476 consistent with somewhat more reducing (e.g., suboxic) conditions during the Rising SPICE (Figs.  
477 5F, 8D). At Duibian, the  $Mo_{EF}$  and  $C_{org}/P$  proxies covary positively ( $r = +0.62$ ,  $n = 69$ ,  $p(\alpha) < 0.05$ )  
478 but lack a significant relationship to  $U_{EF}$  ( $r = -0.01$ ,  $n = 69$ ,  $p(\alpha) > 0.05$ ,  $r = -0.20$ ,  $n = 31$ ,  $p(\alpha) >$   
479  $0.05$ , respectively). We regard  $Mo_{EF}$  and  $C_{org}/P$  as the more reliable redox proxies given the mutual  
480 consistency of their secular patterns and the fact that they indicate more reducing conditions at the  
481 peak of the SPICE, as expected for an event marked by enhanced marine productivity (Zhou et al.,  
482 2015). The pattern of declining  $U_{EF}$  during the mid-SPICE may have some other cause, e.g.,  
483 drawdown of global seawater U concentrations due to expansion of oxygen minimum zones  
484 (OMZs) (cf. Hetzel et al., 2009).

485 The pattern of secular variation in regional seawater redox conditions reconstructed in our  
486 study is independently supported by paired CAS and pyrite sulfur isotope (i.e.,  $\delta^{34}S_{CAS}$  and  
487  $\delta^{34}S_{pyrite}$ ) analyses. The  $\Delta^{34}S_{CAS-pyrite}$  values of both shallow- and deep-water sections from  
488 Laurentia and Gondwana are consistently high ( $\sim 20-40$  ‰) in the late Guzhangian, with a  
489 decrease to a minimum ( $\sim 20$  to  $0$  ‰) in the middle Paibian, followed by a rebound to high values  
490 ( $\sim 20-40$  ‰) in the early Jiangshanian (Gill et al., 2011) (Fig. 9D). This pattern is consistent with a  
491 strong reduction of the seawater sulfate pool during the Rising SPICE, probably as a result of  
492 large-scale pyrite burial and increased amounts of free  $H_2S$  in the water column (Algeo et al.,  
493 2015), reflecting local expansion of shelf anoxia during the late Guzhangian to the middle Paibian  
494 (this study).

495

#### 496 5.2.2. Redox conditions in global ocean

497 The SPICE interval was marked by rising oxygen levels in both the atmosphere and oceans  
498 (Zhang et al., 2022). Atmospheric oxygen levels ( $pO_2$ ) are variously estimated to have risen from  
499  $\sim 5$  to  $10\%$  (Krause et al., 2018) or from  $\sim 15$  to  $25\%$  (Saltzman et al., 2011). This oxygenation  
500 event was driven by massive burial of organic matter, as revealed by a global rise in  $\delta^{13}C_{carb}$  (Gill  
501 et al., 2011), leading to falling atmospheric  $pCO_2$  and climatic cooling. Climatic cooling generally  
502 steepens the equator-to-pole temperature gradient (Barron et al., 1995) and invigorates oceanic  
503 circulation (Cai and Chu, 1998), mainly through intensification of zonal winds rather than oceanic  
504 temperature contrasts (Wunsch, 2002; Huybers and Wunsch, 2010). In the middle-late Cambrian,  
505 a cooler climate promoted global-ocean circulation and deep-ocean ventilation during the Rising

506 SPICE (as revealed by a positive shift in carbonate  $\delta^{238}\text{U}$ ; Dahl et al., 2014) as well as a  
507 concurrent intensification of continent-margin upwelling (Stouffer et al., 2006). Changes in  
508 upwelling intensity were focused along specific continental margins, leading to locally elevated  
509 productivity and organic carbon sinking fluxes and, thus, expanded oxygen minimum zones  
510 (OMZs), despite a general improvement in deep-ocean ventilation. Thus, global-ocean redox  
511 changes during the SPICE event were spatially variable, depending on proximity to  
512 paleo-upwelling zones.

513 Comparison of redox proxy data from the study sections in South China with those for the  
514 globally distributed auxiliary sections (Fig. 1A) demonstrates a systematic pattern of  
515 environmental redox variation during the SPICE event. The Pre-SPICE to Early SPICE intervals  
516 are marked by weaker organic matter burial (thus lower  $\delta^{13}\text{C}_{\text{carb}}$  values) and consequently higher  
517 atmospheric  $p\text{CO}_2$  (thus warmer climate), which led to weakened global-ocean circulation and  
518 depressed marine productivity (cf. Stouffer et al., 2006). This change resulted in expanded  
519 global-ocean hypoxia (e.g., a negative shift in  $\delta^{238}\text{U}$ ; Dahl et al., 2014), while OMZs on shelf  
520 margins contracted (due to low productivity), resulting in mostly oxic conditions on the lower  
521 slope (this study) and a reduction in euxinia (as revealed by decreased enrichments of Mo, U and  
522 V) on the upper slope (Gill et al., 2021). A major redox transition occurred during the Rising  
523 SPICE, when massive organic matter burial (thus higher  $\delta^{13}\text{C}_{\text{carb}}$  values) resulted in declining  
524 atmospheric  $p\text{CO}_2$  and rising  $\text{O}_2$  (Saltzman et al., 2011; Krause et al., 2018). Concurrently,  
525 climatic cooling due to lower  $p\text{CO}_2$  led to improved global-ocean ventilation and oxygenation (i.e.,  
526 first-order positive shifts in  $\delta^{238}\text{U}$ ; Dahl et al., 2014), while elevated marine productivity led to an  
527 expansion of OMZs (i.e., locally more hypoxic conditions in lower slope settings; this study).  
528 Ocean-redox conditions changed again during the Falling SPICE, marked by a contraction of  
529 OMZs in the late Paibian to early Jiangshanian that resulted in a return of oxic conditions to deep  
530 slope facies (e.g., Duibian, this study). This development was probably in response to reduced  
531 marine productivity, as recorded by declining  $\delta^{13}\text{C}$ - $\delta^{34}\text{S}$  of the Falling SPICE interval.

532 Despite commonalities in temporal patterns of redox variation, the study and auxiliary  
533 sections exhibit regionally unique features that may have been due to differences in water depth,  
534 watermass restriction, or regional oceanic circulation (see Supplemental file for facies data and  
535 water-depth interpretations). Compared to the largely oxic conditions observed in South China,  
536 some localities exhibit more intense seawater de-oxygenation. For example, local redox proxy  
537 data (e.g., Fe speciation) for the Andrarum no. 3 core (Alum Shale, Sweden) record dominantly  
538 euxinic conditions during the Pre-SPICE, followed by a shift toward less reducing conditions  
539 (ferruginous) close to the peak of the SPICE, and a return to euxinic conditions during the Falling  
540 and Post-SPICE intervals (Gill et al., 2011, 2021; Dahl et al., 2013). This pattern was punctuated  
541 by short-term (millennial-scale) dysoxic episodes, as inferred from sedimentological and  
542 ichnological data (Egenhoff et al., 2015). The generally more reducing conditions of the Alum  
543 Shale may have been related to stagnation of watermass circulation on the Baltic Craton during the  
544 Cambrian eustatic highstand (Thickpenny, 1987; Høyberget and Bruton, 2008). Moreover, OMZ

545 expansion during the Rising SPICE did not cause enrichments of trace metals (e.g., Mo, U, and V)  
546 in the Alum Shale (Gill et al., 2021), which is consistent with either regional watermass restriction  
547 (cf. Algeo and Maynard, 2008) or a general drawdown of trace metals in the global ocean linked  
548 to expanded anoxia in the Early SPICE interval (cf. Dahl et al., 2014, 2019). A global-ocean redox  
549 proxy record (i.e., carbonate  $\delta^{238}\text{U}$ ) has been generated only for the Mount Whelan core (Australia;  
550 Dahl et al., 2014). It shows an intensification of global-oceanic hypoxia during the Pre-SPICE to  
551 early Rising SPICE, with a shift towards more oxic conditions in the late Rising SPICE, before a  
552 probable re-expansion of anoxic facies during the Falling SPICE, although aspects of these  
553 interpretations are somewhat uncertain owing to the sparsity and unequal temporal distribution of  
554 the  $\delta^{238}\text{U}$  data.

555

### 556 5.3. Global carbon-sulfur cycle changes during the SPICE

557 The marine carbon and sulfur cycles are commonly coupled through biochemical processes  
558 such as photosynthesis and microbial sulfate reduction (Jorgensen, 1982; Mazumdar et al., 2012;  
559 Antler et al., 2013). Major fractionations of carbon and sulfur isotopes are associated with the  
560 production of organic matter from dissolved inorganic carbon (DIC) and pyrite from sulfate  
561 (Bottrell and Newton, 2006). Owing to the long residence times of DIC and sulfate in the ocean  
562 (~100 kyr and ~13 Myr, respectively; Claypool et al., 1980; Zeebe and Wolf-Gladrow, 2001), their  
563 isotopic compositions in seawater generally reflect changes in the burial fluxes of organic matter  
564 and pyrite.

565 During the Early and Rising SPICE, the carbon and sulfur isotopic profiles show general  
566 first-order positive excursions. At Wangcun and Duibian A, the late Guzhangian to middle Paibian  
567 interval (i.e., Units II to III) is characterized by roughly simultaneous positive excursions of  
568  $\delta^{34}\text{S}_{\text{CAS}}$  (~+35 ‰ to ~+50 ‰ and ~+30 ‰ to ~+50 ‰, respectively), and  $\delta^{13}\text{C}_{\text{carb}}$  (~0 ‰ to ~+4 ‰  
569 and ~+1 ‰ to ~+4 ‰, respectively). At Wangcun,  $\delta^{34}\text{S}_{\text{CAS}}$  is positive correlated ( $r = +0.59$ ,  $n = 9$ ,  
570  $p(\alpha) \sim 0.05$ ) to  $\delta^{13}\text{C}_{\text{carb}}$  during the Early SPICE, while no relationship ( $r = -0.43$ ,  $n = 5$ ,  $p(\alpha) >$   
571  $0.05$ ) exists during the Rising SPICE (Fig. 2C-D). At Duibian A, a rise of  $\delta^{34}\text{S}_{\text{CAS}}$  (~+30 ‰ to  
572 ~+45 ‰) corresponds to nearly no changes of  $\delta^{13}\text{C}_{\text{carb}}$  (~+1 ‰) during the Early SPICE, while a  
573 positive correlation is marginally statistically significant ( $r = +0.67$ ,  $n = 7$ ,  $p(\alpha) \sim 0.05$ ) during the  
574 Rising SPICE (Fig. 3C-D). The first-order positive correlation between  $\delta^{34}\text{S}_{\text{CAS}}$  and  $\delta^{13}\text{C}_{\text{carb}}$  during  
575 the Early and Rising SPICE suggests coupling of the global marine carbon and sulfur cycles,  
576 presumably due to co-burial of organic matter and pyrite and a small reservoir of marine sulfate,  
577 driven by elevated marine productivity and expanded shelf/slope hypoxia (Dahl et al., 2014;  
578 Zhang et al., 2022; this study).

579 During the Falling SPICE, the carbon and sulfur isotopic profiles show negative excursions  
580 and intermittent coupling. The late Paibian-early Jiangshanian interval (i.e., Falling SPICE, Unit  
581 IV) is characterized by simultaneous shifts toward lower  $\delta^{13}\text{C}_{\text{carb}}$  and  $\delta^{34}\text{S}_{\text{CAS}}$  values, declining to  
582 minima of ~+1 ‰ and ~+15 to +20 ‰, respectively. The correlations are significant for  $\delta^{34}\text{S}_{\text{CAS}}$  vs.  
583  $\delta^{13}\text{C}_{\text{carb}}$  at Wangcun ( $r = +0.63$ ,  $n = 7$ ,  $p(\alpha) \sim 0.05$ ) and Duibian A ( $r = +0.56$ ,  $n = 14$ ,  $p(\alpha) < 0.05$ ),

584 but not at Duibian B ( $r = +0.17$ ,  $n = 38$ ,  $p(\alpha) > 0.10$ ) (Figs. 2C-D, 3C-D, 4C-D). These differences  
585 may exist owing to regional variation in the net burial rates of organic matter and pyrite, but they  
586 are not inconsistent with reduced marine productivity in South China during the Falling SPICE.

587 In contrast to the SPICE, the Pre-SPICE and Post-SPICE intervals in the study sections are  
588 characterized by non-synchronous variation in  $\delta^{34}\text{S}_{\text{CAS}}$  and  $\delta^{13}\text{C}_{\text{carb}}$ , suggesting a general  
589 decoupling of the global marine carbon and sulfur cycles. In detail, the middle Drumian to middle  
590 Guzhangian interval (i.e., Pre-SPICE, Unit Ib) exhibits fluctuations in  $\delta^{34}\text{S}_{\text{CAS}}$  (from  $\sim +25$  ‰ to  
591  $\sim +35$  ‰) that coincided with little change in  $\delta^{13}\text{C}_{\text{carb}}$  ( $\sim 0$  ‰) at Wangcun (Fig. 2C-D). The early  
592 Jiangshanian interval (i.e., Post-SPICE, Unit IV) exhibits a shift toward lower  $\delta^{13}\text{C}_{\text{carb}}$  values  
593 ( $\sim +1$  ‰) that is decoupled from  $\delta^{34}\text{S}_{\text{CAS}}$  at Wangcun ( $r = -0.07$ ,  $n = 8$ ,  $p(\alpha) > 0.10$ ) and Duibian B  
594 ( $r = +0.44$ ,  $n = 11$ ,  $p(\alpha) > 0.10$ ) (Figs. 2C-D, 3C-D). Thus, variations in marine productivity and  
595 organic carbon and pyrite burial were not sufficiently large in the pre-SPICE and post-SPICE  
596 intervals to override other influences on the global marine carbon and sulfur cycles.

597 All of the auxiliary sections show  $\delta^{13}\text{C}_{\text{carb}}-\delta^{34}\text{S}_{\text{CAS}}$  coupling during the late Guzhangian to  
598 earliest Jiangshanian (i.e., Early to Falling SPICE) and decoupling during the early-middle  
599 Guzhangian (i.e., Pre-SPICE) and early Jiangshanian (i.e., Post-SPICE), conforming to the general  
600 pattern reported here for Wangcun and Duibian. Covariation of  $\delta^{13}\text{C}_{\text{carb}}$  and  $\delta^{34}\text{S}_{\text{CAS}}$  is observed  
601 not only in deep-water sections (e.g., TE-1 Texas County Core, Duibian) but also in  
602 intermediate-depth (e.g., Mount Whelan Core, Shingle Pass) and shallow-water (e.g., Lawson  
603 Cove) sections of Laurentia and Gondwana (Fig. 9). This transregional pattern of carbon-sulfur  
604 cycling confirms marine productivity as the main control on coupled  $\delta^{13}\text{C}_{\text{carb}}-\delta^{34}\text{S}_{\text{CAS}}$  variation  
605 throughout the SPICE event (cf. Dahl et al., 2014). In contrast, the Pre-SPICE and Post-SPICE  
606 intervals were likely associated with a warmer climate, more sluggish oceanic circulation, and  
607 lower (and less variable) marine productivity.

608

#### 609 5.4. Trilobite biodiversity and its relationship to environmental changes during the SPICE event

##### 610 5.4.1. Global comparison of trilobite biodiversity

611 Trilobite biostratigraphic studies from Laurentia resulted in recognition of the EMBE at the  
612 end of the Guzhangian Stage and the ESBE in the early Jiangshanian Stage, each of which  
613 reportedly exhibits two phases of extinction (Longacre, 1970; Palmer, 1965a, 1965b; Stitt, 1971;  
614 Taylor, 2006; Babcock et al., 2017). For the EMBE, the first phase coincided with the base of the  
615 Laurentian *Coosella perplexa* Subzone of the latest Guzhangian (i.e., Early SPICE) and was  
616 marked by the disappearance of the majority of shallow-water trilobites with no concurrent change  
617 in  $\delta^{13}\text{C}_{\text{carb}}$  values (Palmer, 1979; Gerhardt and Gill, 2016). The second phase of the EMBE was  
618 less severe and coincided with the uppermost *C. perplexa* Subzone of the Early Paibian (i.e., onset  
619 of the Rising SPICE), marked by the disappearance of surviving members of the *C. perplexa*  
620 Subzone fauna. Generally, the EMBE is characterized not only by a decline in species diversity  
621 but also by a shift to biofacies that have broader environmental distributions as well as extensive  
622 immigration of taxa from off-shelf and shelf-margin sites to shelf areas (Westrop and Cuggy,

623 1999). The ESBE is relatively less studied than the EMBE, but its first and second phases  
624 coincided with the lowermost *Ir. major* Zone and the *Taenicephalus* Zone of the early  
625 Jiangshanian (i.e., Post-SPICE), respectively. Collectively, these extinctions resulted in a shift in  
626 dominance from the Marjumiid Biome of the Guzhangian to the Pterocephaliid Biome of the  
627 earliest Paibian, and subsequently to the Ptychaspid Biome of the early Jiangshanian (Palmer,  
628 1984; Saltzman et al., 2000) (Fig. 10). Although biomes were first recognized from patterns seen  
629 in Laurentian trilobite faunas, correlative patterns of diversity changes can now be recognized  
630 elsewhere, including in South China (Zhou and Zhen, 2008; Zhang et al., 2021).

631 The trilobite biodiversity curves generated for the present study are only regionally  
632 representative but nonetheless in broad accord with global evolutionary trends during the late  
633 Guzhangian. Thus, although the Marjumiid, Pterocephaliid, and Ptychaspid biomes *sensu stricto*  
634 were endemic to Laurentia (e.g., Saltzman et al., 2000), similar and iterative patterns of trilobite  
635 evolutionary diversification can be seen in age-equivalent successions in South China (Zhang et  
636 al., 2021; this study), making these biomes *sensu lato* of global significance. In the present study,  
637 the first phase of the EMBE is recognizable as a decrease in trilobite range-through species  
638 diversity from  $\sim 10$  to 1 at Wangcun (i.e., at  $\sim 230$ - $270$  m) and from  $\sim 25$  to  $\sim 5$  at Duibian (i.e., at  
639  $\sim -4$  to  $+1$  m), during an interval of nearly constant or slightly positive-shifted  $\delta^{13}\text{C}_{\text{carb}}$  values (i.e.,  
640 Early SPICE) (Fig. 10A, D). A similar decline in trilobite diversity without a major carbon isotope  
641 excursion has been reported from strata in Laurentia that are age-equivalent to the Early SPICE  
642 interval (Palmer, 1979, 1984; Gerhardt and Gill, 2016) (Fig. 10E). This observation suggests that  
643 the trilobite diversity curves in the present study are globally representative (cf. Zhou and Zhen,  
644 2008; Zhang et al., 2021), and that the EMBE was a widespread event triggered by global  
645 environmental changes during the Early SPICE interval.

646 The newly generated trilobite diversity curves for the Rising SPICE interval at both Wangcun  
647 and Duibian are regionally representative (see Zhang et al., 2021). Although a gradual increase in  
648 trilobite diversity occurred immediately after the EMBE in Laurentia (Fig. 10E; Palmer, 1984;  
649 Rowell and Brady, 1976), our study reveals a trend toward lower diversity at  $\sim 1$ - $30$  m in Duibian  
650 A, coincident with an increase of  $\delta^{13}\text{C}_{\text{carb}}$  and stable  $\delta^{34}\text{S}_{\text{CAS}}$  values during the Rising SPICE,  
651 reaching a minimum of one species at the peak of the SPICE (Fig. 10D). A drop in taxonomic  
652 diversity during the Rising SPICE was also reported from the Paibi section (which is the GSSP of  
653 the base of the Furongian Series and Paibian Stage),  $\sim 50$  km southwest of Wangcun (Peng et al.,  
654 2004; Zhang et al., 2021). However, a recent study from South China inferred approximately  
655 constant trilobite diversity during the Rising SPICE, before a decline during the Falling SPICE  
656 (Zhang et al., 2021).

657 The trilobite biodiversity curves from the present study are in accord with documented  
658 evolutionary trends for the Jiangshanian of South China (Zhou and Zhen, 2008; Zhang et al.,  
659 2021), which may be representative of contemporaneous global patterns. Trilobite species  
660 diversity remained at a higher level through the end of the SPICE, before declining during the  
661 ESBE at the transition to the Post-SPICE interval (Palmer, 1979, 1984; Zhou and Zhen, 2008; this

662 study). Biodiversity changes in South China are comparable to those reported from correlative  
663 units in Laurentia (Fig. 10D-E), although, as with the EMBE, the existence of two separate  
664 extinction pulses during the ESBE has not been recognized in the present study sections.

665 Proposed triggers for the EMBE include cooling climate/seawater (e.g., climatic cooling, rise  
666 of permanent thermocline, and upwelling of cool nutrient-rich waters) (Õpik, 1966;  
667 Lochman-Balk, 1970; Stitt, 1975; Perfetta et al., 1999; Elrick et al., 2011), and seawater anoxia  
668 and/or euxinia (Saltzman et al., 1998; Hurtgen et al., 2009; Gill et al., 2011; Dahl et al., 2014). In  
669 contrast, the environmental controls on the ESBE have received little consideration to date. Below,  
670 we consider possible environmental controls on the EMBE and ESBE, based on a combination of  
671 previous studies and our new paleontological and geochemical data.

672

#### 673 5.4.2. End-Marjuman Biome Extinction (EMBE)

674 The cause of the extinction of the Marjumiid Biome (*sensu lato*) and the spread of the  
675 Pterocephaliid Biome (*sensu lato*) over shelf areas during the Early SPICE has long been  
676 debated. Early work focused on differences in the preferred habitats of these two biomes  
677 (Palmer, 1984; Pratt, 1992). The fauna of the Marjumiid Biome mostly occupied shallow-water  
678 sandstone and siltstone facies close to paleo-shorelines, resulting in relatively high degrees of  
679 endemism. In contrast, the fauna of the Pterocephaliid Biome was better represented in  
680 deeper-water, shale-rich facies beneath the oceanic thermocline, allowing it to migrate globally  
681 and develop into a eurytopic assemblage (Pratt, 1992). More recent work has focused on the role  
682 of temperature change, with climatic cooling, a rise of the permanent thermocline, and/or  
683 upwelling of deep waters being proposed as the trigger for the EMBE (Palmer, 1984; Saltzman et  
684 al., 2000; Elrick et al., 2011). Whereas the Marjumiid Biome favored warmer waters, the  
685 Pterocephaliid Biome, and especially its agnostoid elements and olenimorphic morphotypes,  
686 preferred cooler, deeper waters (Fortey and Owens, 1990), although one of its members, the genus  
687 *Erixanium*, had a narrow latitudinal range centered on the paleo-Equator (Lu and Lin, 1989; Stitt  
688 et al., 1994; Zhou and Zhen, 2008), suggesting a preference for warmer temperatures (Hughes,  
689 2000). At Duibian, representatives of the Pterocephaliid Biome comprise a low-diversity fauna  
690 dominated by proceratopygine and iwayaspine species (Lu and Lin, 1989; Hughes and Rushton,  
691 1990; Peng et al. 2012) that may have been especially tolerant of challenging or variable  
692 environmental conditions linked to oxygen stress (cf. Zhang et al., 2021). This fauna yielded to the  
693 Ptychaspiid Biome, which was characterized by a decline in endemic species and an increase in  
694 more cosmopolitan elements (Cook and Taylor, 1975; Żylińska, 2001, 2002; Álvaro et al., 2013).  
695 Taxa appearing immediately after the ESBE include both the widespread and arguably pelagic  
696 genus *Irvingella* (Fortey, 1985), which was adept at crossing open ocean basins, and the more  
697 typical “ptychopariid” *Maladoidella*, which was restricted to shallow-shelf settings along the  
698 margin of Gondwana (Rushton and Hughes, 1996) but spanned an unusually wide range of  
699 paleolatitudes (Hughes, 2000). Such widespread occurrence along the Gondwanan margin may  
700 attest to a reduced latitudinal temperature gradient following the ESBE, possibly associated with

701 global warming. The biotic succession in the present study sections is thus consistent with cooling  
702 in conjunction with the EMBE followed by warming in association with the ESBE.

703 The biotic extinctions during the Early SPICE may have been analogous to the extinction  
704 events at the onset and termination of the Hirnantian Glaciation of the Late Ordovician, about 50  
705 Myr later (Algeo et al., 2016). The <1-Myr-long Hirnantian Glaciation was marked by a ~5 °C  
706 decline of global temperatures (Trotter et al., 2008; Finnegan et al., 2011), a ~70-150 m sea-level  
707 fall (Brenchley et al., 2003; Finnegan et al., 2011), and a ~4-6 ‰ positive  $\delta^{13}\text{C}$  excursion (i.e., the  
708 Hirnantian carbon isotope excursion or HICE, Bergström et al., 2006). An extinction of  
709 warm-water faunas at the onset of this glacial episode (Barash, 2014) and its replacement by the  
710 cool-water-adapted *Hirnantia* Fauna (Zhan et al., 2010; Rasmussen and Harper, 2011) were  
711 possibly analogous to the transition from the warm-water Marjumiid Biome to the cool-water  
712 Pterocephaliid Biome during the Early SPICE (Palmer, 1984; Pratt, 1992).

713 The role of temperature change as a control on trilobite biomes during the middle-late  
714 Cambrian has been inadequately tested to date using oxygen-isotope data. Phosphatic brachiopod  
715  $\delta^{18}\text{O}$  from western Laurentia provided evidence of a climate cooling event during the Pre-SPICE,  
716 followed by climate warming during the Rising SPICE (Elrick et al., 2011). However, this pattern  
717 is likely to represent only a local signal linked to shallowing of a tropical shelf as a result of global  
718 sea-level fall (Fig. 10F), shifting the local watermass from the cooler thermocline into the warmer  
719 surface layer of the ocean during the SPICE. The EMBE was followed by the rise of the  
720 cool-water Pterocephaliid Biome fauna in western Laurentia (Stitt, 1975; Rowell and Brady,  
721 1976; Palmer, 1984), which is inconsistent with the general climatic warming inferred by Elrick et  
722 al. (2011). However, global climate cooling is likely to have prevailed during the SPICE, as  
723 evidenced by sedimentological, stratigraphic, and geochemical records (e.g., greater burial  
724 sequestration of organic matter, and thus a reduced greenhouse effect) (Saltzman, 2005; Cherns  
725 and Wheeley, 2009; Sørensen et al., 2020) (Fig. 10I).

726 Redox changes are likely to have contributed to trilobite biome turnovers, although the  
727 extinction of the Marjumiid Biome during the latter part of the Early SPICE lagged a major  
728 negative shift in carbonate  $\delta^{238}\text{U}$  during its earlier part (Dahl et al., 2014; note: some uncertainty  
729 linked to limited fossil data from Whelan core), suggesting that transient expansion of  
730 global-ocean hypoxia was not the proximate cause of the EMBE. Rather, the EMBE may have  
731 been due to the impact of global-ocean circulation changes on regional redox conditions. Global  
732 climatic cooling is likely to have led to an expansion of seawater hypoxia on shelf margins subject  
733 to upwelling, where nutrient-rich deepwaters enhanced regional productivity and organic carbon  
734 sinking fluxes, producing locally more reducing conditions (cf. Whitney et al., 2005; Stouffer et al.,  
735 2006). This hypothesis is consistent with a concurrent improvement in global-ocean ventilation  
736 during the Early SPICE and Rising SPICE, as evidenced by first-order positive shifts of carbonate  
737  $\delta^{238}\text{U}$  (Dahl et al., 2014). The present study provides evidence of OMZ expansion as shown by a  
738 transition from oxic to suboxic waters on the Jiangnan Slope of South China during the Rising  
739 SPICE (Fig. 10C). This redox change is likely to have placed outer-shelf trilobite communities

740 under stress despite generally improved ventilation of the global ocean. The extinction of  
741 indigenous cool-water trilobites belonging to the early Paibian Pterocephaliid Biome in  
742 deep-slope settings supports our inference of OMZ expansion and increased shelf anoxia as the  
743 principal control on the EMBE and the subsequent reduced diversity of the Pterocephaliid  
744 Biome (cf. Pratt, 1992), as does the nature of the trilobites that dominate the Paibian fauna (see  
745 above). During the latter part of the Falling SPICE, contraction of OMZs on shelf margins  
746 permitted local increases in the abundance and diversity of the Pterocephaliid Biome fauna  
747 *sensu lato* prior to the ESBE (Fig. 10D).

748

#### 749 5.4.3. End-Steptoean Biome Extinction (ESBE)

750 The causes of the ESBE remain uncertain. Given that the ESBE occurred at the end of a  
751 period of global carbon cycle instability, this biotic event is likely to have been related to the  
752 attenuation of environmental disturbances associated with the carbon cycle. The ESBE was  
753 probably related to global climate change but evidence for this is presently scant. Biopateite  
754 oxygen isotopes suggest that in Laurentia, the Falling and Post-SPICE episodes corresponded to a  
755 cooling climate (Elrick et al., 2011), although cooling may have been due to local water-column  
756 deepening as a result of global warming and continental ice mass decay. Global climate change  
757 during the ESBE has not been studied to date. If the ESBE is analogous to the extinction of the  
758 *Hirnantia* Fauna at the termination of the Hirnantian Glaciation, then it may also have been  
759 associated with global climatic warming (Fig. 10I). However, environmental factors controlling  
760 the ESBE were probably not simply the opposite of those influencing the EMBE (e.g., climate  
761 warming as opposed to earlier climate cooling), because there are cosmopolitan taxa among both  
762 the latest Paibian and early Jiangshanian biomes (e.g., *Hedinaspis*, *Irvingella*, and *Maladoidella*  
763 at Duibian; Peng et al., 2012).

764 The spatial scale of seawater redox changes during the ESBE requires consideration. As oxic  
765 seawater conditions persisted during this time interval throughout the study area, local redox  
766 changes cannot explain this extinction event (Fig. 10C). Widespread seawater anoxia may have  
767 developed in the global ocean during this interval, as indicated by rapid increases in  $\delta^{34}\text{S}_{\text{CAS}}$  and  
768  $\Delta^{34}\text{S}_{\text{CAS-pyrite}}$  in both South China and Laurentia (Fig. 9). However, the geographic extent of  
769 oceanic redox changes remains to be tested via a proxy suitable for addressing global trends (e.g.,  
770 carbonate U isotopes).

771

## 772 6. Conclusions

773 Paired  $\delta^{13}\text{C}_{\text{carb}}$ - $\delta^{34}\text{S}_{\text{CAS}}$  profiles and trilobite species diversity curves spanning the lower  
774 Drumian to lower Jiangshanian were generated for a shallow-water succession at Wangcun and a  
775 deep-water succession at Duibian, located on the Jiangnan Slope in South China. Enrichment  
776 factors for U and Mo, along with  $C_{\text{org}}/P$  ratios, suggest mostly oxic conditions in the study sections  
777 during the SPICE event, except hypoxic (i.e., suboxic) seawater conditions from the earliest  
778 Paibian to the middle Paibian (i.e., Rising SPICE) at Duibian.  $\delta^{13}\text{C}_{\text{carb}}$  was tightly coupled with

779  $\delta^{34}\text{S}_{\text{CAS}}$  during the late Guzhangian to late Paibian, demonstrating first-order control of  
780 contemporaneous environmental changes by the marine carbon cycle. Local  $\delta^{13}\text{C}_{\text{carb}}$  trends mirror  
781 positive excursions of  $\sim 3\%$  found globally during the Rising SPICE, which were driven by  
782 elevated global marine productivity and enhanced burial of organic matter. The major positive  
783 excursion in  $\delta^{34}\text{S}_{\text{CAS}}$  started earlier than that of  $\delta^{13}\text{C}_{\text{carb}}$  during the Early SPICE, and  $\delta^{34}\text{S}_{\text{CAS}}$   
784 remained stable during the Rising SPICE before declining during the Falling SPICE. The Falling  
785 SPICE was characterized by diminished global marine productivity, resulting in reduced co-burial  
786 of organic matter and pyrite. In order to investigate the global marine carbon-sulfur cycles during  
787 the SPICE event, we further compiled  $\delta^{13}\text{C}_{\text{carb}}-\delta^{34}\text{S}_{\text{CAS}}$  variations in four shallow- to deep-water  
788 successions on the slope/continental margin of Laurentia and Gondwana. The relationship  
789 between  $\delta^{13}\text{C}_{\text{carb}}$  and  $\delta^{34}\text{S}_{\text{CAS}}$  in these settings is similar to that at Wangcun and Duibian,  
790 suggesting globally consistent patterns of carbon-sulfur cycling during the SPICE event.

791 The local trilobite species diversity curves are comparable to those from Laurentia, showing a  
792 major decline in biodiversity during the End-Marjuman Biomere Extinction (EMBE) in the Early  
793 SPICE, as well as the End-Steptoean Biomere Extinction (ESBE) in the Post-SPICE. Therefore,  
794 the SPICE event should be extended downwards to include the Early SPICE interval of the late  
795 Guzhangian Stage, in a manner that more clearly links the EMBE to the SPICE. We further  
796 evaluated effects of climate change, global and local seawater redox conditions on these biotic  
797 extinctions, and propose that expansion of seawater hypoxia on shelf margins as a result of global  
798 climate cooling, invigorated global ocean circulation, and intensified continent-margin upwelling  
799 may have directly contributed to the extinction of the trilobite fauna of the Marjumiid Biomere  
800 during the Early SPICE, and the attenuation of those environmental changes during the Falling  
801 SPICE set the stage for the subsequent extinction of the Pterocephaliid Biomere.

802

### 803 **Acknowledgments**

804 We thank Science Editors Brad Singer and Rob Strachan for handling this manuscript, and  
805 we thank Associate Editor Bradley D. Cramer and two anonymous reviewers for their constructive  
806 comments. We thank Ziheng Li, Guoxiong Ou and Ziliang Wan for their help in the field and  
807 laboratory. This study is supported by NSFC grants (42073073, 92055212, 41977264, 41930322,  
808 41825019, 41803011, 41821001, 42130208), the Fundamental Research Funds for the Central  
809 Universities, China University of Geosciences–Wuhan (CUGCJ1815, CUGQYZX1728), and the  
810 MOST Special Fund (MSF-GPMR2022-7) of the State Key Laboratory of Geological Processes  
811 and Mineral Resources, China University of Geosciences, Wuhan. TWD thanks the Carlsberg  
812 Foundation (CF16-0876) for financial support. This is a contribution to IGCP668, and N.C.H.  
813 acknowledges NSF EAR-1849963.

814

### 815 **References**

816 Algeo, T.J., and Ingall, E., 2007, Sedimentary  $\text{C}_{\text{org}}:\text{P}$  ratios, paleocean ventilation, and Phanerozoic  
817 atmospheric  $\text{pO}_2$ : *Palaeogeogr. Palaeoclimatol. Palaeoecol.*, v. 256, p. 130–155.

- 818 Algeo, T.J., and Li, C., 2020, Redox classification and calibration of redox thresholds in  
819 sedimentary systems: *Geochimica et Cosmochimica Acta*, v. 287, p. 8–26.
- 820 Algeo, T.J., and Liu, J.S., 2020, A re-assessment of elemental proxies for paleoredox analysis:  
821 *Chem. Geol.*, v. 540, p. 119549.
- 822 Algeo, T.J., and Maynard, J.B., 2008, Trace-metal covariation as a guide to water-mass conditions  
823 in ancient anoxic marine environments: *Geosphere*, v. 4, p. 872-887.
- 824 Algeo T.J., and Tribovillard N., 2009, Environmental analysis of paleoceanographic systems based  
825 on molybdenum–uranium covariation: *Chem. Geol.*, v. 268, p. 211–225.
- 826 Algeo, T.J., Rowe, H., Hower, J. C., Schwark, L., Herrmann, A., and Heckel, P., 2008, Changes in  
827 ocean denitrification during Late Carboniferous glacial–interglacial cycles: *Nature*  
828 *Geoscience*, v. 1, p. 709–714.
- 829 Algeo, T.J., Luo, G.M., Song, H.Y., Lyons, T.W., and Canfield, D.E., 2015, Reconstruction of  
830 secular variation in seawater sulfate concentrations: *Biogeosciences*, v. 12, p. 2131-2151.
- 831 Algeo, T.J., Marengo, P.J., and Saltzman, M.R., 2016, Co-evolution of oceans, climate, and the  
832 biosphere during the ‘Ordovician Revolution’: a review: *Palaeogeography, Palaeoclimatology,*  
833 *Palaeoecology*, v. 458, p. 1–11.
- 834 Al-Husseini, M.I., 2017, Late Cambrian SPICE and Ice. 12 pp. [www.orbitalscale.com](http://www.orbitalscale.com).
- 835 Álvaro, J.J., Ahlberg, P., Babcock, L.E., Bordonaro, O. L., Choi, D.K., Cooper, R.A., Ergaliev,  
836 G., Kh., Gapp, I., Ghobadi Pour, M., Hughes, N.C., Jago, J.B., Korovnikov, I., Laurie, J.R.,  
837 Lieberman, B.S., Paterson, J.R., Pegel, T.V., Popov, L.E., Rushton, A.W.A., Sukhov, S.S.,  
838 Tortello, M.F., Zhou, Z.-Y., and Žyli ű ska, A., 2013, Global Cambrian trilobite  
839 palaeobiogeography assessed using parsimony analysis of endemism, *in* Harper, D.A.T., and  
840 Servais, T., eds., *Early Palaeozoic Palaeobiogeography and Palaeogeography*, Geological  
841 Society of London, Memoir 38, p. 273–296.
- 842 Anderson, R.F., Fleisher, M.Q., and LeHuray, A.P., 1989, Concentration, oxidation state, and  
843 particulate flux of uranium in the Black Sea: *Geochimica et Cosmochimica Acta*, v. 53, p.  
844 2215–2224.
- 845 Antler, G., Turchyn, A.V., Rennie, V., Herut, B., and Sivan, O., 2013, Coupled sulfur and oxygen  
846 isotope insight into bacterial sulfate reduction in the natural environment: *Geochimica et*  
847 *Cosmochimica Acta*, v. 118, p. 98–117.
- 848 Babcock, L.E., Peng, S., and Ahlberg, P., 2017, Cambrian trilobite biostratigraphy and its role in  
849 developing an integrated history of the Earth system: *Lethaia*, v. 50, p. 381–399.
- 850 Baker, J.L., 2010, Carbon isotopic fractionation across a late Cambrian carbonate platform: a  
851 regional response to the SPICE event as recorded in the Great Basin, United States [M.S.  
852 thesis]: Las Vegas, University of Nevada, 681 pp.
- 853 Barash, M.S., 2014, Mass extinction of the marine biota at the Ordovician-Silurian transition due  
854 to environmental changes: *Oceanology*, v. 54, p. 780–787.
- 855 Barron, E.J., Fawcett, P.J., Peterson, W.H., Pollard, D. and Thompson, S.L., 1995, A “simulation”  
856 of mid - Cretaceous climate: *Paleoceanography*, v. 10, p. 953-962.
- 857 Bergström, S.M., Saltzman, M.M., and Schmitz, B., 2006, First record of the Hirnantian (Upper

858 Ordovician)  $\delta^{13}\text{C}$  excursion in the North American midcontinent and its regional implications:  
859 Geological Magazine, v. 143, p. 657–678.

860 Bottrell, S.H., and Newton, R.J., 2006, Reconstruction of changes in global sulfur cycling from  
861 marine sulfate isotopes: Earth Science Reviews, v. 75, p. 59–83.

862 Brand, U., 2004, Carbon, oxygen and strontium isotopes in Paleozoic carbonate components: an  
863 evaluation of original seawater-chemistry proxies: Chem. Geol., v. 204, p. 23–44.

864 Brenchley, P.J., Carden, G.A., Hints, L., Kaljo, D., Marshall, J.D., Martma, T., and Nölvak, J.,  
865 2003, High-resolution stable isotope stratigraphy of Upper Ordovician sequences: constraints  
866 on the timing of bioevents and environmental changes associated with mass extinction and  
867 glaciation: Geological Society of America Bulletin, v. 115, p. 89–104.

868 Cai, W., and Chu, P.C., 1998, Oceanic responses to gradual transitions of equator-to-pole  
869 temperature-gradients: Quarterly Journal of the Royal Meteorological Society, v. 124, p.  
870 2817–2828.

871 Cherns, L., and Wheeley, J.R., 2009, Early Palaeozoic cooling events: Peri-Gondwana and beyond.  
872 In: Bassett, M.G. (ed.) Early Palaeozoic Peri-Gondwana Terranes, New Insights from  
873 Tectonics and Biogeography: Geological Society of London, Special Publication, v. 325, p.  
874 257–278.

875 Claypool, G.E., Holser, W.T., Kaplan, I.R., Sakai, H., and Zak, I., 1980, The age curves for sulfur  
876 and oxygen isotopes in marine sulfate and their mutual interpretation: Chemical Geology, v.  
877 28, p. 199–260.

878 Cook, H.E., and Taylor, M.E., 1975, Early Paleozoic continental margin sedimentation, trilobite  
879 biofacies, and the thermocline, western United States: Geology, v. 3, p. 559–562.

880 Dahl, T.W., Boyle, R.A., Canfield, D.E., Connelly, J.N., Gill, B.C., Lenton, T.M., and Bizzarro, M.,  
881 2014, Uranium isotopes distinguish two geochemically distinct stages during the later  
882 Cambrian SPICE event: Earth Planet. Sci. Lett., v. 401, p. 313–326.

883 Dahl, T.W., Ruhl, M., Hammarlund, E.U., Canfield, D.E., Rosing, M.T., Bjerrum, C.J., 2013,  
884 Tracing euxinia by molybdenum concentrations in sediments using handheld X-ray  
885 fluorescence spectroscopy (HHXRF): Chemical Geology, v. 360, p. 241–251.

886 Dahl, T.W., Siggaard-Andersen, M.L., Schovsbo, N.H., Persson, D.O., Husted, S., Hougård, I.W.,  
887 Dickson, A.J., and Nielsen, A.T., 2019, Brief oxygenation events in locally anoxic oceans  
888 during the Cambrian solves the animal breathing paradox: Scientific Reports, v. 9, p. 1–9.

889 Dronov, A., and Popov, L.E., 2004, Traces of frost action in the Obolus-Sand: The evidence for  
890 sub-glacial climate in the mid-Cambrian to early Ordovician (Tremadocian) of the east Baltic  
891 (abstract). In: Munnecke, A., Servais, T., Schulbert, C. (eds) Early Palaeozoic  
892 Palaeogeography and Palaeoclimate: Erlanger Geologische Abhandlungen, v. 5, 32 pp.

893 Edwards, C.T., Fike, D.A., and Saltzman, M.R., 2019, Testing carbonate-associated sulfate (CAS)  
894 extraction methods for sulfur isotope stratigraphy: A case study of a Lower–Middle  
895 Ordovician carbonate succession, Shingle Pass, Nevada, USA: Chemical Geology, v. 529,  
896 119297.

- 897 Egenhoff, S.O., Fishman, N.S., Ahlberg, P., Maletz, J., Jackson, A., Kolte, K., Lowers, H., Mackie,  
898 J., Newby, W., and Petrowsky, M., 2015, Sedimentology of SPICE (Steptoean positive  
899 carbon isotope excursion): a high-resolution trace fossil and microfabric analysis of the  
900 middle to late Cambrian Alum Shale Formation, southern Sweden. In: Larsen, D., Egenhoff,  
901 S.O., Fishman, N.S. (eds.), *Paying Attention to Mudrocks: Priceless!*: Geol. Soc. Am. Spec.  
902 Pap., v. 515, p. 87–102.
- 903 Elrick, M., Rieboldt, S., Saltzman, M., and McKay, R.M., 2011, Oxygen-isotope trends and  
904 seawater temperature changes across the Late Cambrian Steptoean positive carbon-isotope  
905 excursion (SPICE event): *Geology*, v. 39, p. 987–990.
- 906 Feng, Z.Z., Peng, Y.M., Jin, Z.K., and Bao, Z.D., 2002, Lithofacies Palaeogeography of the  
907 Middle Cambrian. *China Journal of Palaeogeography*, v. 4, p. 1–11.
- 908 Finnegan, S., Bergmann, K., Eiler, J.M., Jones, D.S., Fike, D.A., Eisenman, I., Hughes, N.C.,  
909 Tripathi, A.K., and Fischer, W.W., 2011, The magnitude and duration of Late Ordovician-Early  
910 Silurian glaciation: *Science*, v. 331, p. 903–906.
- 911 Fortey, R.A., 1985, Pelagic trilobites as an example of deducting life habits in extinct arthropods:  
912 *Transactions of the Royal Society of Edinburgh*, v. 76, p. 219-230.
- 913 Fortey, R.A., and Owens, R.M., 1990. Evolutionary radiations in the Trilobita: In *Major evolutionary*  
914 *radiations*, p. 139-164.
- 915 Gerhardt, A.M., and Gill, B.C., 2016, Elucidating the relationship between the later Cambrian  
916 end-Marjuman extinctions and SPICE Event: *Palaeogeography Palaeoclimatology*  
917 *Palaeoecology*, v. 461, p. 362–373.
- 918 Gill, B.C., Lyons, T.W., and Saltzman, M.R., 2007, Parallel, high-resolution carbon and sulfur  
919 isotope records of the evolving Paleozoic marine sulfur reservoir: *Palaeogeogr.*  
920 *Palaeoclimatol. Palaeoecol.*, v. 256, p. 156–173.
- 921 Gill, B.C., Lyons, T.W., Young, S.A., Kump, L.R., Knoll, A.H., and Saltzman, M.R., 2011,  
922 Geochemical evidence for widespread euxinia in the later Cambrian ocean: *Nature*, v. 469, p.  
923 80–83.
- 924 Gill, B.C., Dahl, T.W., Hammarlund, E.U., LeRoy, M.A., Gordon, G.W., Canfield, D.E., Anbar,  
925 A.D., and Lyons, T.W., 2021, Redox dynamics of later Cambrian oceans: *Palaeogeography,*  
926 *Palaeoclimatology, Palaeoecology*, v. 581, 110623.
- 927 Hammer, Ø., and Svensen, H.H., 2017, Biostratigraphy and carbon and nitrogen geochemistry of  
928 the SPICE event in Cambrian low-grade metamorphic black shale, Southern Norway:  
929 *Palaeogeogr. Palaeoclimatol. Palaeoecol.*, v. 468, p. 216–227.
- 930 Hetzel, A., Böttcher, M.E., Wortmann, U.G., and Brumsack, H.J., 2009, Paleo-redox conditions  
931 during OAE 2 reflected in Demerara Rise sediment geochemistry (ODP Leg  
932 207): *Palaeogeography, Palaeoclimatology, Palaeoecology*, v. 273, p. 302–328.
- 933 Høyberget, M., and Bruton, D.L., 2008, Middle Cambrian trilobites of the suborders *Agnostina*  
934 and *Eodiscina* from the Oslo Region, Norway: *Palaeontogr. Abt. A*, v. 286, p. 1–87.

- 935 Hughes, N. C., 2000, Ecologic evolution of Cambrian trilobites. pp. 370-403. *In* Zhuravlev, A.Y. &  
 936 Riding, R., Eds. *The Ecology of the Cambrian Radiation*: Columbia University Press, New  
 937 York.
- 938 Hughes, N.C., and Rushton, A.A., 1990, Computer-aided restoration of a Late Cambrian  
 939 ceratopygid trilobite from Wales, and its phylogenetic implications: *Palaeontology*, v. 33, p.  
 940 429–445.
- 941 Hurtgen, M.T., Pruss, S.B., and Knoll, A.H., 2009, Evaluating the relationship between the carbon  
 942 and sulfur cycles in the later Cambrian ocean: an example from the Port au Port Group,  
 943 western Newfoundland, Canada: *Earth Planet. Sci. Lett.*, v. 281, p. 288–297.
- 944 Huybers, P., and Wunsch, C., 2010, Paleophysical oceanography with an emphasis on transport  
 945 rates: *Annual Review of Marine Science*, v. 2, p. 1-34.
- 946 Krause, A.J., Mills, B.J., Zhang, S., Planavsky, N.J., Lenton, T.M., and Poulton, S.W., 2018,  
 947 Stepwise oxygenation of the Paleozoic atmosphere: *Nature Communications*, v. 9, p. 1–10.
- 948 Jorgensen, B.B., 1982, Mineralisation of organic matter in the sea bed—the role of sulphate  
 949 reduction: *Nature*, v. 296, p. 643–645.
- 950 Lee, J.H., Chen, J., and Chough, S.K., 2015, The middle–late Cambrian reef transition and related  
 951 geological events: a review and new view: *Earth-Sci. Rev.*, v. 145, p. 66–84.
- 952 Li, D.D., Zhang, X.L., Hu, D.P., Chen, X.Y., Huang, W., Zhang, X., Li, M.H., Qin, L.P., Peng,  
 953 S.C., and Shen, Y.A., 2018, Evidence of a large  $\delta^{13}\text{C}_{\text{carb}}$  and  $\delta^{13}\text{C}_{\text{org}}$  depth gradient for  
 954 deep-water anoxia during the late Cambrian SPICE event: *Geology*, v. 46, p. 631–634.
- 955 Lochman-Balk, C., 1970, Upper Cambrian faunal patterns on the craton: *Geol. Soc. Am. Bull.*, v.  
 956 81, p. 3197-3224.
- 957 Longacre, S.A., 1970, Trilobites of the Upper Cambrian Ptychaspid Biome Wilberns Formation,  
 958 Central Texas: *Paleontol. Soc. Mem.*, v. 44, p. 1–68.
- 959 Lu, Y.H., and Lin, H.L., 1989, The Cambrian trilobites of western Zhejiang: *Palaeontologia*  
 960 *Sinica*, v. 178(25), 287 pp.
- 961 Marengo, P.J., Corsetti, F.A., Kaufman, A.J., and Bottjer, D.J., 2008, Environmental and  
 962 diagenetic variations in carbonate associated sulfate: an investigation of CAS in the lower  
 963 Triassic of the western USA: *Geochim. Cosmochim. Acta*, v. 72, p. 1570–1582.
- 964 Marshall, C.R., 2006, Explaining the Cambrian “explosion” of animals: *Ann. Rev. Earth Planet.*  
 965 *Sci.*, v. 34, p. 355–384.
- 966 Marshall, J.D., 1992, Climatic and oceanographic isotopic signals from the carbonate rock record  
 967 and their preservation: *Geological Magazine*, v. 129, p. 143–160.
- 968 Matthews, R.K., and Al-Husseini, M.I., 2010, Orbital-forcing glacio-eustasy: A  
 969 sequence-stratigraphic time scale: *GeoArabia*, v. 15, p. 155–167.
- 970 Mazumdar, A., Peketi, A., Joao, H., Dewangan, P., Borole, D.V., and Kocherla, M., 2012,  
 971 Sulfidization in a shallow coastal depositional setting: Diagenetic and palaeoclimatic  
 972 implications: *Chemical Geology*, v. 322-323, p. 68–78.
- 973 McLennan, S.M., 2001. Relationships between the trace element composition of sedimentary  
 974 rocks and upper continental crust: *Geochem. Geophys. Geosyst.* 2 (2000GC000109, 24 pp.).

- 975 Moysiuk, J., and Caron, J.B., 2019, Burgess Shale fossils shed light on the agnostid problem:  
976 Proceedings of the Royal Society B, v. 286(1894), p. 20182314.
- 977 Öpik, A.A., 1966, The Early Upper Cambrian crisis and its correlation: J. Proc. Roy. Soc. New  
978 South Wales, v. 100, p. 9–14.
- 979 Palmer, A.R., 1965a, Biomere: A new kind of biostratigraphic unit: J. Paleontol., v. 39, p. 149–  
980 153.
- 981 Palmer, A.R., 1965b, Trilobites of the Late Cambrian Pterocephaliid Biomere in the Great Basin,  
982 United States: Geol. Surv. Prof. Pap., v. 493, 153 pp.
- 983 Palmer, A.R., 1979, Biomere boundaries re-examined: Alcheringa, v. 3, p. 33–41.
- 984 Palmer, A.R., 1984, The biomere problem — evolution of an idea: J. Paleontol., v. 58, p. 599–611.
- 985 Peng, S.C., 2005, Potential candidate stratotypes for the levels of *Lejopyge laevigata* and  
986 *Agnostotes orientalis*: Acta Micropaleontologica Sinica, v. 22, p. 148–149.
- 987 Peng, S.C., and Robison, R.A., 2000, Agnostoid biostratigraphy across the Middle-Upper  
988 Cambrian boundary in China: Paleontological Society Memoir 53, Journal of Paleontology,  
989 v. 74, Supplement p. 1–104.
- 990 Peng, S.C., Babcock, L.E., and Lin, H.L., 2004, Polymerid trilobites from the Cambrian of  
991 northwestern Hunan, China, volume 1: Corynexochida, Lichida, and Asaphida, Beijing,  
992 Science Press, 333 pp.
- 993 Peng, S.C., Babcock, L. E., and Lin, H.L., 2005, Polymerid trilobites from the Cambrian of  
994 northwestern Hunan, China, volume 2: Ptychopariida, Eodiscida, and Undetermined forms,  
995 Beijing, Science Press, 355 pp.
- 996 Peng, S.C., Babcock, L., Robison, R., Lin, H.L., Rees, M., and Saltzman, M., 2004, Global  
997 standard stratotype-section and point (GSSP) of the Furongian Series and Paibian Stage  
998 (Cambrian): Lethaia, v. 37, p. 365–379.
- 999 Peng, S.C., Babcock, L.E., Zuo, J.X., Lin, H.L., Zhu, X.J., Yang, X.F., Robison, R.A., Qi, Y.P., and  
1000 Bagnoli, G., 2006, Proposed GSSP for the base of Cambrian Stage 7, coinciding with the first  
1001 appearance of *Lejopyge laevigata*, Hunan, China: Palaeoworld, v. 15, p. 367–383.
- 1002 Peng, S.C., Babcock, L.E., Zuo, J.X., Lin, H.L., and Chen, Y.A., 2009, The Global Boundary  
1003 Stratotype Section and Point (GSSP) of the Guzhangian Stage (Cambrian) in the Wuling  
1004 Mountains, Northwestern Hunan, China: Episodes, v. 32, p. 41–55.
- 1005 Peng, S.C., Babcock, L.E., and Cooper, R.A., 2012, The Cambrian Period, pp. 437–488. In:  
1006 Gradstein, F.M., Ogg, J.G., Schmitz, M.D., Ogg, G.M. (eds.), The Geologic Time Scale 2012:  
1007 Elsevier, New York.
- 1008 Perfetta, P.J., Shelton, K.L., and Stitt, J.H., 1999, Carbon isotope evidence for deep-water invasion  
1009 at the Marjumiid-Pterocephaliid biomere boundary, Black Hills, USA: A common origin for  
1010 biotic crises on Late Cambrian shelves: Geology, v. 27, p. 403–406.
- 1011 Pratt, B.R., 1992, Trilobites of the Marjuman and Steptoean stages (Upper Cambrian),  
1012 Rabbitkettle Formation, southern Mackenzie Mountains, northwest Canada: Palaeontogr.  
1013 Canad., v. 9, 179 pp.

- 1014 Present, T.M., Gutierrez, M., Paris, G., Kerans, C., Grotzinger, J.P., and Adkins, J.F., 2019,  
1015 Diagenetic controls on the isotopic composition of carbonate-associated sulphate in the  
1016 Permian Capitan Reef Complex, West Texas: *Sedimentology*, v. 66, p. 2605–2626.
- 1017 Pulsipher, M.A., Schiffbauer, J.D., Jeffrey, M.J., Huntley, J.W., Fike, D.A., and Shelton, K.L.,  
1018 2021, A meta-analysis of the Steptoean positive carbon isotope excursion: The SPICEraq  
1019 database: *Earth-Science Reviews*, v. 212, p. 103442.
- 1020 Rasmussen, C.M.Ø., and Harper, D.A.T., 2011, Interrogation of distributional data for the End  
1021 Ordovician crisis interval: Where did disaster strike?: *Geological Journal*, v. 46, p. 478–500.
- 1022 Rasmussen, C.M.Ø., Kröger, B., Nielsen, M.L., Colmenar, J., 2019, Cascading trend of Early  
1023 Paleozoic marine radiations paused by Late Ordovician extinctions: *Proc. Natl. Acad. Sci.*  
1024 *USA*, v. 116, p. 7207–7213.
- 1025 Richardson, J.A., Lepland, A., Hints, O., Prave, A. R., Gilhooly III, W.P., Bradley, A.S., and Fike,  
1026 D.A., 2021, Effects of early marine diagenesis and site-specific depositional controls on  
1027 carbonate-associated sulfate: Insights from paired S and O isotopic analyses: *Chemical*  
1028 *Geology*, v. 584, p. 120525.
- 1029 Richardson, J.A., Newville, M., Lanzirotti, A., Webb, S.M., Rose, C.V., Catalano, J.G., and Fike,  
1030 D. A., 2019, Depositional and diagenetic constraints on the abundance and spatial variability  
1031 of carbonate-associated sulfate: *Chemical Geology*, v. 523, p. 59-72.
- 1032 Rieboldt, S.E., 2005, Inarticulate Brachiopods of the late Maijumiid and Pteroccephaliid Biomes  
1033 (late Middle- early Late Cambrian) of West-Central Utah and East-Central Nevada, U.S.A.  
1034 [Ph.D. thesis]: Berkeley, University of California, 311 pp.
- 1035 Rowell, A.J., and Brady, M.J., 1976, Brachiopods and biomes: *Brigham Young Univ. Geol.*  
1036 *Studies*, v. 23, p. 165–180.
- 1037 Runkel, A.C., McKay, R.M., and Palmer, A.R., 1998, Origin of a classic cratonic sheet sandstone:  
1038 Stratigraphy across the Sauk II–Sauk III boundary in the Upper Mississippi Valley:  
1039 *Geological Society of America Bulletin*, v. 110, p. 188–210.
- 1040 Rushton, A. W. A., and Hughes, N. C., 1996, Biometry, systematics and biogeography of the late  
1041 Cambrian trilobite *Maladoidella abdita*: *Transactions of the Royal Society of Edinburgh:*  
1042 *Earth Sciences*, v. 86, p. 247–256.
- 1043 Saltzman, M.R., 2005, Phosphorus, nitrogen, and the redox evolution of the Paleozoic oceans:  
1044 *Geology*, v. 33, p. 573–576.
- 1045 Saltzman, M.R., and Thomas, E., 2012, Carbon isotope stratigraphy, pp. 207-232. In: Gradstein,  
1046 F.M., Ogg, J.G., Schmitz, M.D., Ogg, G.M., eds., *The Geologic Time Scale 2012*: Elsevier,  
1047 New York.
- 1048 Saltzman, M.R., Runnegar, B., and Lohmann, K.C., 1998, Carbon isotope stratigraphy of Upper  
1049 Cambrian (Steptoean Stage) sequences of the eastern Great Basin: Record of a global  
1050 oceanographic event: *Geol. Soc. Am. Bull.*, v. 110, p. 285–297.
- 1051 Saltzman, M.R., Ripperdan, R.L., Brasier, M.D., Lohmann, K.C., Robison, R.A., Chang, W.T.,  
1052 Peng, S., Ergaliev, E.K., and Runnegar, B., 2000, A global carbon isotope excursion (SPICE)

1053 during the Late Cambrian: relation to trilobite extinctions, organic-matter burial and sea level:  
1054 Palaeogeogr. Palaeoclimatol. Palaeoecol., v. 162, p. 211–223.

1055 Saltzman, M.R., Cowan, C.A., Runkel, A.C., Runnegar, B., Stewart, M.C., and Palmer, A.R., 2004,  
1056 The Late Cambrian SPICE ( $\delta^{13}\text{C}$ ) event and the Sauk II–Sauk III regression: new evidence  
1057 from Laurentian Basins in Utah, Iowa, and Newfoundland: *J. Sed. Res.*, v. 74, p. 365–377.

1058 Saltzman, M.R., Young, S.A., Kump, L. R., Gill, B.C., Lyons, T.W., Runnegar, B., and Berner,  
1059 R.A., 2011, Pulse of atmospheric oxygen during the Late Cambrian: *Proc. Natl. Acad. Sci.*  
1060 USA, v. 108, p. 3876–3881.

1061 Schiffbauer, J.D., Huntley, J.W., Fike, D.A., Jeffrey, M.J., Gregg, J.M., and Shelton, K.L., 2017,  
1062 Decoupling biogeochemical records, extinction, and environmental change during the  
1063 Cambrian SPICE event: *Sci. Adv.*, v. 3, e1602158.

1064 Schrag, D.P., Higgins, J.A., Macdonald, F.A., and Johnston, D.T., 2013, Authigenic carbonate and  
1065 the history of the global carbon cycle: *Science*, v. 339, p. 540–543.

1066 Scott, C., Lyons, T.W., 2012. Contrasting molybdenum cycling and isotopic properties in euxinic  
1067 versus non-euxinic sediments and sedimentary rocks: Refining the paleoproxies: *Chem. Geol.*,  
1068 v. 324, p. 19–27.

1069 Servais, T., Lehnert, O., Li, J., Mullins, G.L., Munnecke, A., Nuetzel, A., and Vecoli, M., 2008,  
1070 The Ordovician Biodiversification: revolution in the oceanic trophic chain: *Lethaia*, v. 41, p.  
1071 99–109.

1072 Servais, T., Owen, A.W., Harper, D.A., Kröger, B., and Munnecke, A., 2010, The Great  
1073 Ordovician Biodiversification Event (GOBE): the palaeoecological dimension: *Palaeogeogr.*  
1074 *Palaeoclimatol. Palaeoecol.*, v. 294, p. 99–119.

1075 Sørensen, A.L., Nielsen, A.T., Thibault, N., Zhao, Z., Schovsbo, N.H., and Dahl, T.W., 2020,  
1076 Astronomically forced climate change in the late Cambrian: *Earth and Planetary Science*  
1077 *Letters*, v. 548, 116475.

1078 Stitt, J.H., 1971, Repeating evolutionary pattern in Late Cambrian trilobite biomes: *J. Paleontol.*,  
1079 v. 45, p. 178–181.

1080 Stitt, J.H., 1975, Adaptive radiation, trilobite paleoecology and extinction, Ptychaspidid Biome,  
1081 Late Cambrian of Oklahoma: *Fossils and Strata*, v. 4, p. 381–390.

1082 Stitt, J. H., Rucker, J. D., Boyer, N. D., and Hart, W. D., 1994, New *Elvinia* Zone (Upper  
1083 Cambrian) trilobites from new localities in the Collier Shale, Ouachita Mountains,  
1084 Arkansas: *Journal of Paleontology*, v. 68, p. 518–523.

1085 Stouffer, R.J., Yin, J., Gregory, J.M., Dixon, K.W., Spelman, M.J., Hurlin, W., Weaver, A.J., Eby,  
1086 M., Flato, G.M., Hasumi, H., Hu, A., Jungclaus, J.H., Kamenkovich, I.V., Levermann, A.,  
1087 Montoya, M., Murakami, S., Nawrath, S., Oka, A., Peltier, W.R., Robitaille, D.Y., Sokolov,  
1088 A., Vettoretti, G., and Weber, S.L., 2006, Investigating the causes of the response of the  
1089 thermohaline circulation to past and future climate changes: *J. Clim.*, v. 19, p. 1365–1387.

1090 Swart, P.K., 2008, Global synchronous changes in the carbon isotopic composition of carbonate  
1091 sediments unrelated to changes in the global carbon cycle: *Proceedings of the National*

- 1092 Academy of Sciences, v. 105, p. 13741–13745.
- 1093 Swart, P.K., 2015, The geochemistry of carbonate diagenesis: The past, present and future:  
1094 Sedimentology, v. 62, p. 1233–1304.
- 1095 Swart, P.K., and Kennedy, M.J., 2012, Does the global stratigraphic reproducibility of  $\delta^{13}\text{C}$  in  
1096 Neoproterozoic carbonates require a marine origin? A Pliocene–Pleistocene comparison:  
1097 Geology, v. 40, p. 87–90.
- 1098 Taylor, J.F., 2006, History and status of the biomere concept: Assoc. Australas. Paleontol. Mem.  
1099 32, p. 247–265.
- 1100 Thickpenny, A., 1987, Palaeo-oceanography and depositional environment of the Scandinavian  
1101 Alum Shales: sedimentological and geochemical evidence: Marine clastic sedimentology.  
1102 Springer, Dordrecht, p. 156–171.
- 1103 Trotter, J.A., Williams, I.S., Barnes, C.R., Lecuyer, C., and Nicoll, R.S., 2008, Did cooling oceans  
1104 trigger Ordovician biodiversification? evidence from conodont thermometry: Science, v. 321,  
1105 p. 550–554.
- 1106 Westrop, S.R., 1988, Trilobite diversity patterns in an Upper Cambrian stage: Paleobiology, v. 14,  
1107 p. 401–409.
- 1108 Westrop, S.R., and Cuggy, M.B., 1999, Comparative paleoecology of Cambrian trilobite  
1109 extinctions: J. Paleontol., v. 73, p. 337–354.
- 1110 Westrop, S.R., and Ludvigsen, R., 1987, Biogeographic control of trilobite mass extinction at an  
1111 Upper Cambrian "biomere" boundary: Paleobiology, v. 13, p. 84–99.
- 1112 Whitney, F.A., Crawford, W.R., and Harrison, P.J., 2005, Physical processes that enhance nutrient  
1113 transport and primary productivity in the coastal and open ocean of the subarctic NE Pacific.  
1114 Deep-Sea Res. II, v. 52, p. 681–706.
- 1115 Wotte, T., Shields-Zhou, G.A., and Strauss, H., 2012, Carbonate-associated sulfate: Experimental  
1116 comparisons of common extraction methods and recommendations toward a standard  
1117 analytical protocol: Chemical Geology, v. 326, p. 132–144.
- 1118 Wotte, T., Skovsted, C.B., Whitehouse, M.J., and Kouchinsky, A., 2019, Isotopic evidence for  
1119 temperate oceans during the Cambrian explosion: Scientific Reports, v. 9, 6330, 9 pp.
- 1120 Wunsch, C., 2002, What is the thermohaline circulation?: Science, v. 298, p. 1179–1181.
- 1121 Zeebe R.E., and Wolf-Gladrow D.A., 2001,  $\text{CO}_2$  in Seawater: Equilibrium, Kinetics, Isotopes:  
1122 Elsevier Oceanography Series, 346 pp.
- 1123 Zhan, R.B., Liu, J.B., Percival, I.G., Jin, J.S., and Guipeng, L.L., 2010, Biodiversification of Late  
1124 Ordovician *Hirnantia* fauna on the Upper Yangtze Platform, South China: Science China D:  
1125 Earth Sciences, v. 53, p. 1800–1810.
- 1126 Zhao, M.Y., Zheng, Y.F., and Zhao, Y.Y., 2016, Seeking a geochemical identifier for authigenic  
1127 carbonate: Nature communications, v. 7, p. 1–7.
- 1128 Zhang, L., Algeo, T.J., Zhao, L.S., Chen, Z.Q., Zhao, H., Zhang, Z.H., and Li, C., 2022, Linkage  
1129 of the late Cambrian microbe-metazoan transition (MMT) to shallow-marine oxygenation  
1130 during the SPICE event. Global and Planetary Change, v. 213, p. 103798.
- 1131 Zhang, S.H., Fan, J.X., Morgan, C.A., Henderson, C.M., and Shen, S.Z., 2021, Quantifying the

1132 middle-late Cambrian trilobite diversity pattern in South China: *Palaeogeography,*  
 1133 *Palaeoclimatology, Palaeoecology*, v. 570, p. 110361.

1134 Zhang, Y.G., Yang, T., Hohl, S.V., Zhu, B., He, T.C., Pan, W.Q., Chen, Y.Q., Yao, X.Z., and Jiang,  
 1135 S.Y., 2020, Seawater carbon and strontium isotope variations through the late Ediacaran to  
 1136 late Cambrian in the Tarim Basin: *Precamb. Res.*, v. 345, p. 105769.

1137 Zhou, L., Algeo, T.J., Shen, J., Hu, Z.F., Gong, H.M., Xie, S.C., Huang, J.H., and Gao, S., 2015,  
 1138 Changes in marine productivity and redox conditions during the Late Ordovician Hirnantian  
 1139 glaciation: *Palaeogeography, Palaeoclimatology, Palaeoecology*, v. 420, p. 223–234.

1140 Zhou, Z.Y., and Zhen, Y.Y., 2008, *Trilobite Record of China*: Beijing, Science Press, 401 pp.

1141 Zhu, M.Y., Yang, A.H., Yuan, J.L., Li, G.X., Zhang, J.M., Zhao, F.C., Ahn, S., and Miao, L.Y.,  
 1142 2018, Cambrian integrative stratigraphy and timescale of China: *Sci. China D: Earth Sci.*, v.  
 1143 62, p. 25–60.

1144 Zuo, J., Peng, S., Qi, Y., Zhu, X., Bagnoli, G., and Fang, H., 2018, Carbon-isotope excursions  
 1145 recorded in the Cambrian system, South China: Implications for mass extinctions and  
 1146 sea-level fluctuations: *Journal of Earth Science*, v. 29, p. 479–491.

1147 Żylińska, A., 2001, Late Cambrian trilobites from the Holy Cross Mountains, central Poland: *Acta*  
 1148 *Geologica Polonica*, v. 51, p. 333–383.

1149 Żylińska, A., 2002, Stratigraphic and biogeographic significance of Late Cambrian trilobites from  
 1150 Lysogóry (Holy Cross Mountains, central Poland): *Acta Geologica Polonica*, v. 52, p. 217–  
 1151 238.

1152  
 1153  
 1154

1155 **Figure captions:**

1156  
 1157 Fig. 1. Paleogeographic maps of the Late Cambrian world (A), South China Craton (B), and local  
 1158 maps of Guzhang County (C) and Jiangshan urban area (D), showing locations of Wangcun,  
 1159 Duibian A and B, and other globally distributed SPICE sections discussed in the text. Map A is  
 1160 from <https://deeptimemaps.com> authorized by Colorado Plateau Geosystems Inc. Map B is  
 1161 adapted from Li et al. (2018).

1162

1163 Fig. 2. Trilobite and isotopic data for the Wangcun section: (A) trilobite species ranges, (B)  
 1164 trilobite species diversity; (C) carbonate (carb)  $\delta^{13}\text{C}$  (‰ VPDB); and (D) carbonate-associated  
 1165 sulfate (CAS)  $\delta^{34}\text{S}$  (‰ CDT). In panel A, trilobite range data are from Peng et al. (2009), with red  
 1166 and blue lines representing actual range and range-through data, respectively. The base of the  
 1167 Paibian and the base of the Jiangshanian have been correlated from Duibian A based on  
 1168 trilobite-carbon isotope biochemostratigraphy from Zuo et al. (2018). The gray fields represent the  
 1169 stratigraphic extent of SPICE; ‘Early SPICE’ is newly defined herein, and its base implies an  
 1170 earlier onset of the SPICE than inferred in some earlier studies (see Section 2.5). Abbreviations: *A.*  
 1171 *inexpectans* = *Agnostus inexpectans*; *Ag. orientalis* = *Agnostotes orientalis*; *C. plumula* =  
 1172 *Corynexochus plumula*; *E. rectang.* = *Erixanum rectangularis*; *G. reticulatus* = *Glyptagnostus*

1173 *reticulatus*; *G.s.* = *Glyptagnostus stolidotus*; *Go.n.* = *Goniagnostus nathorsti*; *L.a.* = *Lejopyge*  
1174 *armata*; *Li.r.* = *Linguagnostus reconditus*; *L.l.* = *Lejopyge laevigata*; *Pa.* = *Ptychagnostus*  
1175 *aculeatus*; *Pp.* = *Ptychagnostus punctuosus*; *Pr.b.* = *Proagnostus bulbosus*; *E.* = *Erixanium*; *Ir.* =  
1176 *Irvingella*; *T.* = *Tomagnostella*; Jiangshan. = Jiangshanian; Wu. = Wuliuan.

1177

1178 Fig. 3. Trilobite and isotopic data for the Duibian A section: (A) trilobite species ranges, (B)  
1179 trilobite species diversity; (C) carbonate (carb)  $\delta^{13}\text{C}$  (‰ VPDB); and (D) carbonate-associated  
1180 sulfate (CAS)  $\delta^{34}\text{S}$  (‰ CDT). Trilobite data from Peng et al. (2012). See Figure 2 caption for other  
1181 details.

1182

1183 Fig. 4. Trilobite and isotopic data for the Duibian B section: (A) trilobite species ranges, (B)  
1184 trilobite species diversity; (C) carbonate (carb)  $\delta^{13}\text{C}$  (‰ VPDB); and (D) carbonate-associated  
1185 sulfate (CAS)  $\delta^{34}\text{S}$  (‰ CDT). Trilobite data from Peng et al. (2012). See Figure 2 caption for other  
1186 details.

1187

1188 Fig. 5. Trilobite and elemental data for the Wangcun section: (A) trilobite species diversity; (B)  
1189 total organic carbon (TOC); (C)  $\text{Al}_2\text{O}_3$ ; (D)  $U_{\text{EF}}$ ; (E)  $Mo_{\text{EF}}$ ; and (F)  $C_{\text{org}}/P$ . Red circles represent  
1190 samples with low detrital content ( $\text{Al}_2\text{O}_3 < 1\%$ ) that may result in artificially high  $U_{\text{EF}}$  and  $Mo_{\text{EF}}$   
1191 values. For abbreviations refer to Figure 2.

1192

1193 Fig. 6. Trilobite and elemental data for the Duibian A section: (A) trilobite species diversity; (B)  
1194 total organic carbon (TOC); (C)  $\text{Al}_2\text{O}_3$ ; (D)  $U_{\text{EF}}$ ; (E)  $Mo_{\text{EF}}$ ; and (F)  $C_{\text{org}}/P$ . For other details see  
1195 Figure 5 caption; for abbreviations refer to Figure 2.

1196

1197 Fig. 7. Trilobite and elemental data for the Duibian B section: (A) trilobite species diversity; (B)  
1198 total organic carbon (TOC); (C)  $\text{Al}_2\text{O}_3$ ; (D)  $U_{\text{EF}}$ ; (E)  $Mo_{\text{EF}}$ ; and (F)  $C_{\text{org}}/P$ . For other details see  
1199 Figure 5 caption; for abbreviations refer to Figure 2.

1200

1201 Fig. 8. Seawater redox conditions in Wangcun, Duibian A and B sections, based on (A-C)  $Mo_{\text{EF}}$  vs.  
1202  $U_{\text{EF}}$  and (D) TOC vs. P. Panels A-C are after Algeo and Tribovillard (2009);  $U_{\text{EF}}$  values are mostly  
1203 3-10 in suboxic, and  $Mo_{\text{EF}}$  values  $> 10$  in anoxic environments. Redox thresholds in panel D are  
1204 after Algeo and Ingall (2007);  $C_{\text{org}}:P$  ratios are mostly  $< 50$  in oxic, 50 to 100-125 in suboxic and  
1205 100-125 in anoxic environments. In panel D, all data are shown without reference to  $\text{Al}_2\text{O}_3$  content,  
1206 because the  $C_{\text{org}}:P$  proxy is independent of  $\text{Al}_2\text{O}_3$  content.

1207

1208 Fig. 9. Global comparisons of (A)  $\delta^{13}\text{C}_{\text{carb}}$  (‰ VPDB), (B)  $\delta^{34}\text{S}_{\text{CAS}}$  (‰ CDT), (C)  $\delta^{34}\text{S}_{\text{pyrite}}$  (‰  
1209 CDT), and (D)  $\Delta^{34}\text{S}_{(\text{CAS-py})}$  profiles. Data sources: Shingle Pass (Saltzman et al., 1998; Gill et al.,  
1210 2007); Lawson Cove and TE-1 Texas County Core (Gill et al., 2011); Mount Whelan Core  
1211 (Saltzman et al., 2000; Gill et al., 2011); Wangcun, Duibian A and B (this study). All profiles were  
1212 replotted and smoothed using the Drumian-Guzhangian (~500.5 Ma), Guzhangian-Paibian (~497  
1213 Ma), and Paibian-Jiangshanian (~494 Ma) boundaries as age tie-points, and assuming isochroneity  
1214 of the SPICE peak globally. For sections containing incomplete Guzhangian or Jiangshanian  
1215 stages, age assignments were made assuming a constant sedimentation rate based on the Paibian  
1216 stage. Notes: (1) peak  $\delta^{34}\text{S}_{\text{CAS}}$  values occurred during the Rising SPICE (Gill et al., 2011; this

1217 study); (2) for Shingle Pass, maximum  $\delta^{13}\text{C}_{\text{carb}}$  is reached slightly below a facies change, so the  
1218 peak SPICE interval may have been truncated (Saltzman et al., 2000; Gill et al., 2011). Color  
1219 scheme: green = surface layer, blue = intermediate water depth, and black = deep layer. Note  
1220 existence of a depth-related gradient for each isotopic system. See the Supplemental file for  
1221 descriptions of the sedimentary settings of the sections analyzed here.

1222

1223 Fig. 10. Summary figure for regional and global marine proxies during the SPICE event: (A)  
1224  $\delta^{13}\text{C}_{\text{carb}}$  (‰ VPDB), (B)  $\delta^{34}\text{S}_{\text{CAS}}$  (‰ CDT), (C) seawater redox, and (D) trilobite diversity of South  
1225 China (this study); (E) trilobite diversity of Laurentia, based on House Range (Utah), Highland  
1226 Range (Nevada), Desert Range (Nevada) and Royer Ranch (Oklahoma) sections (Palmer, 1978,  
1227 1984); (F) sea-level changes of Laurentia, based on studies in Upper Mississippi Valley (Runkel et  
1228 al., 1998); (G) seawater redox conditions of Baltica, based on studies of Mo-U enrichments and Fe  
1229 speciation in Andrarum-3 drillcore (Gill et al., 2011); (H) global seawater redox conditions, based  
1230 on studies of carbonate U-isotopes in Whelan no. 1 drillcore, Australia (Dahl et al., 2014); and (I)  
1231 general global SSTs, based on studies of Saltzman (2005), Matthews and Al-Husseini (2010) and  
1232 Al-Husseini (2017). In panels D and E, colors refer to Pre- and Early SPICE vs. Rising and Falling  
1233 SPICE vs. Post-SPICE. In panel E, blue horizontal lines are counted diversity from Palmer (1984).  
1234 In panels D and E, due to lack of biostratigraphic constraints (Palmer, 1984), correlations of  
1235 trilobite diversity curves are based on diversity peaks. For abbreviations see Figures 2-4.

1236

Figure 1

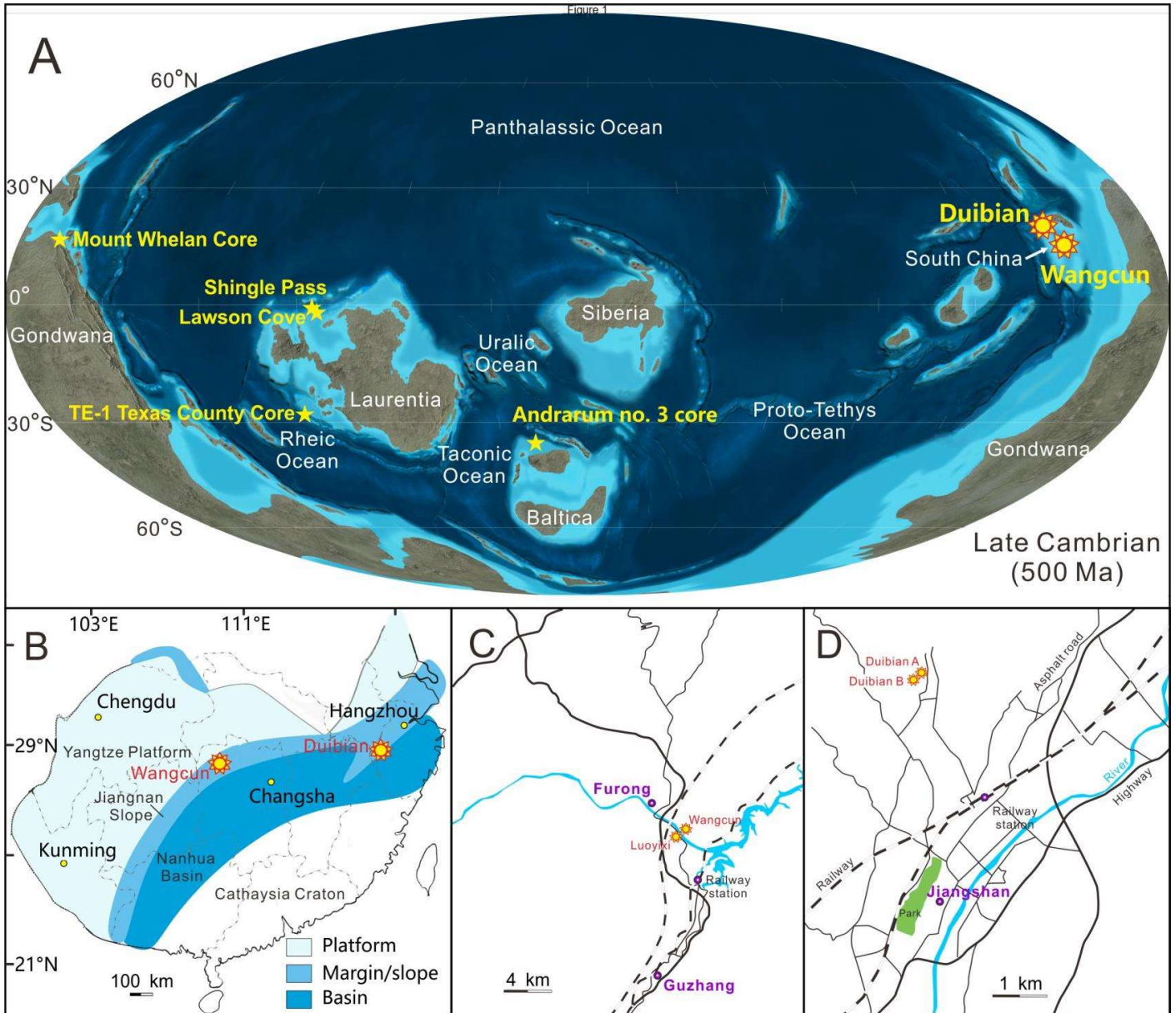


Figure 2

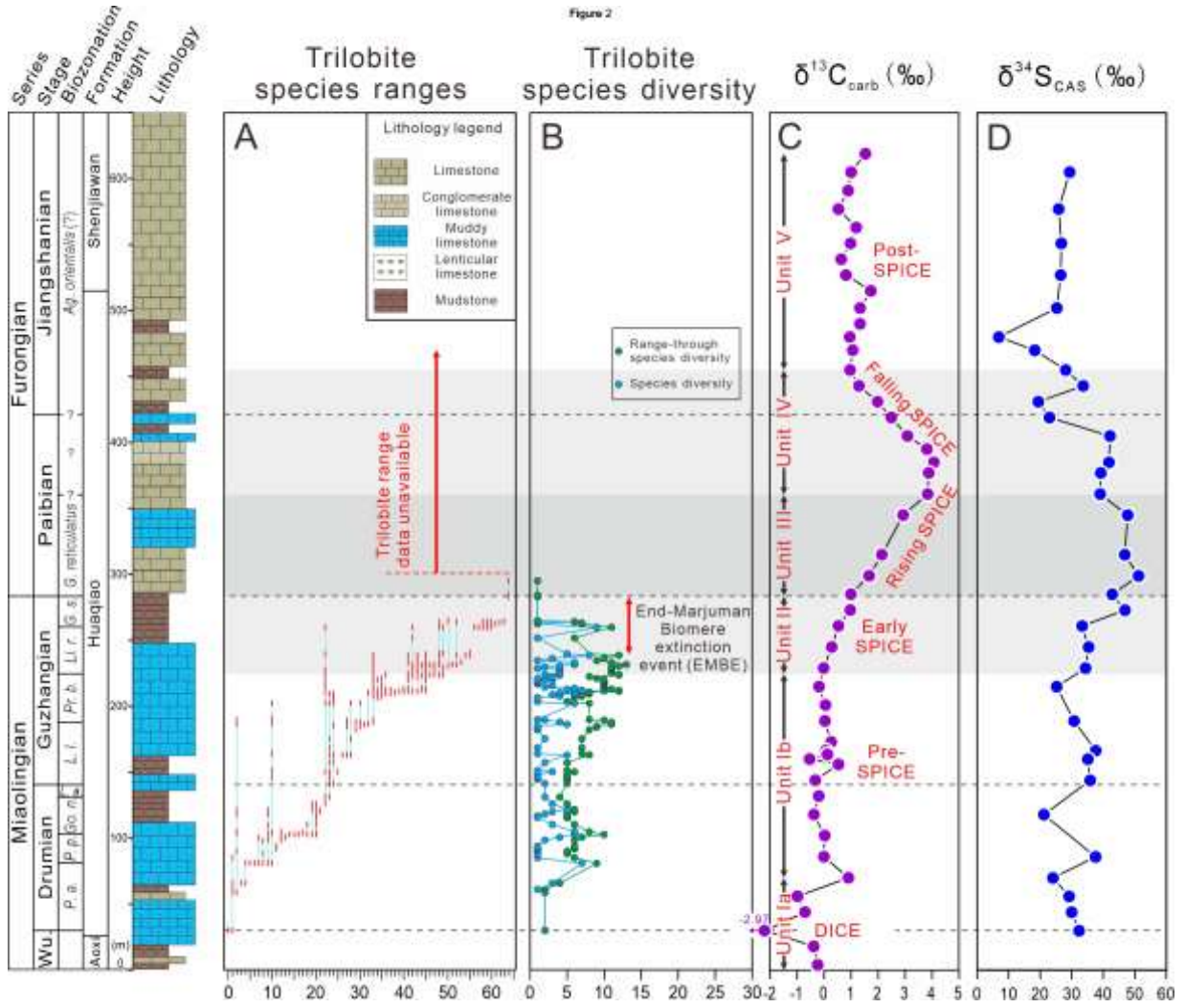


Figure 3

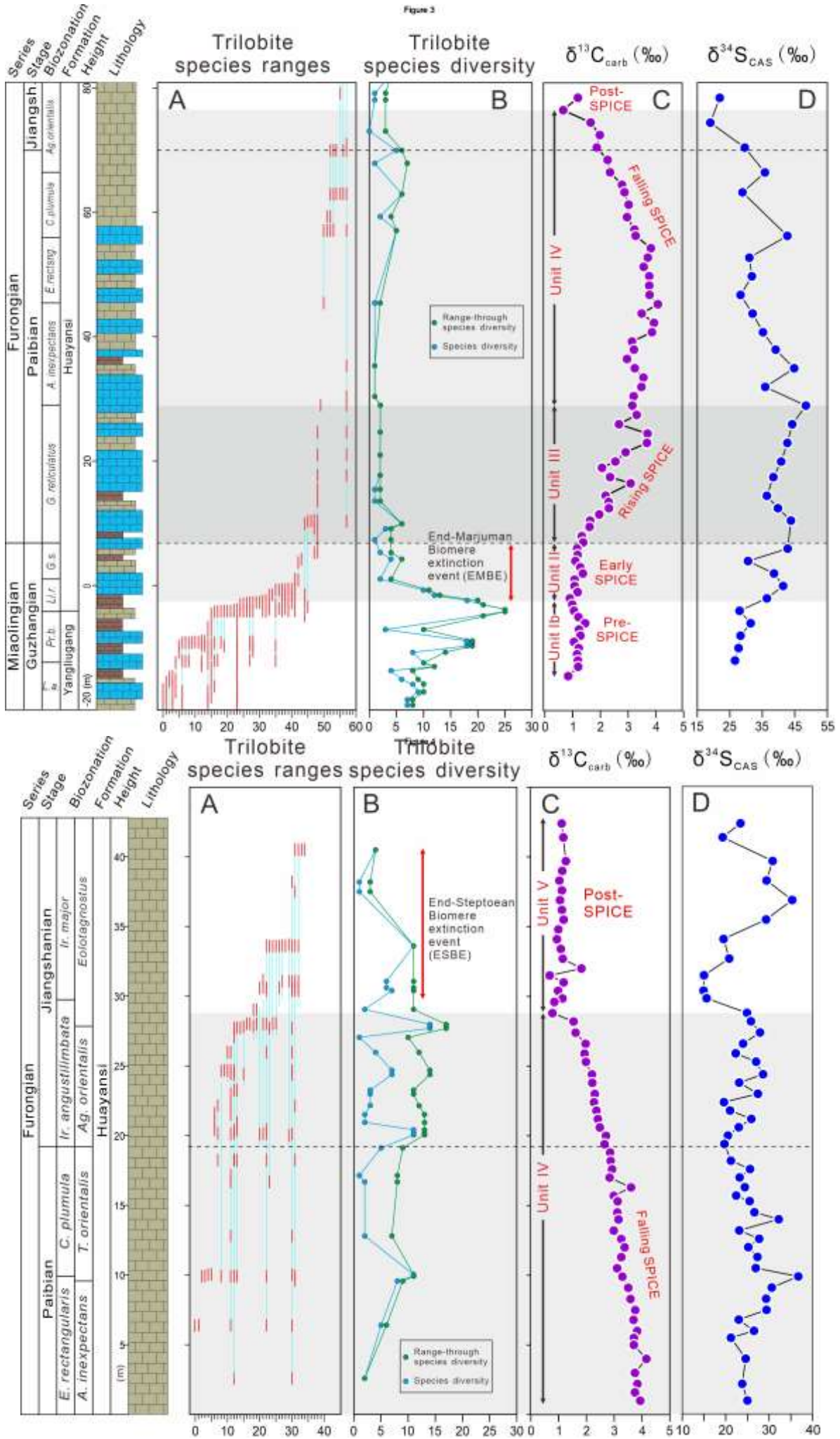


Figure 5

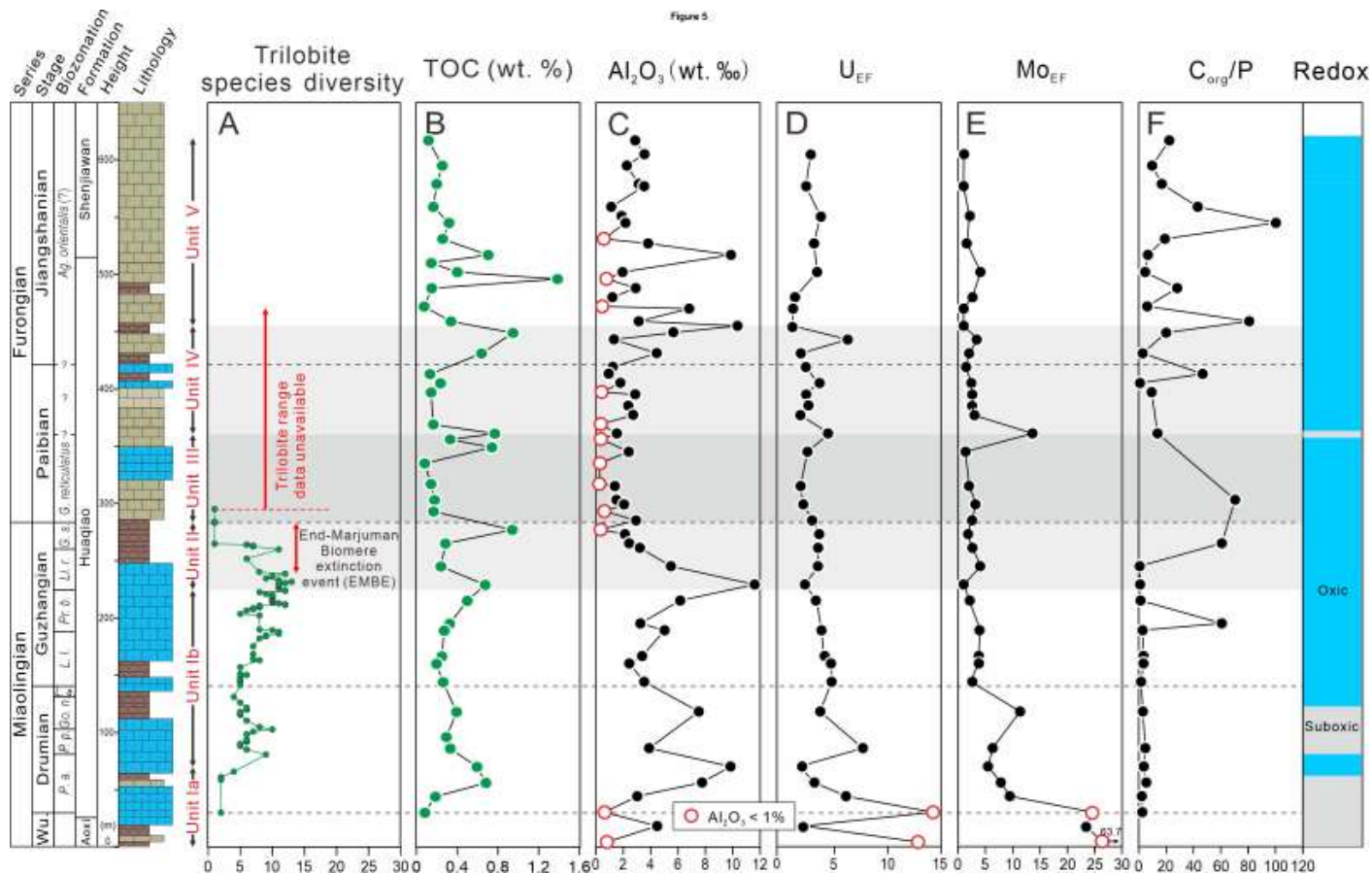


Figure 6

